Journal Pre-proof

Graphdiyne nanoradioprotector with efficient free radical scavenging ability for mitigating radiation-induced gastrointestinal tract damage

Jiani Xie, Chengyan Wang, Ning Wang, Shuang Zhu, Linqiang Mei, Xiao Zhang, Yuan Yong, Lele Li, Chunying Chen, Changshui Huang, Zhanjun Gu, Yuliang Li, Yuliang Zhao

Please cite this article as: Xie J, Wang C, Wang N, Zhu S, Mei L, Zhang X, Yong Y, Li L, Chen C, Huang C, Gu Z, Li Y, Zhao Y, Graphdiyne nanoradioprotector with efficient free radical scavenging ability for mitigating radiation-induced gastrointestinal tract damage, *Biomaterials* (2020), doi: https://doi.org/10.1016/j.biomaterials.2020.119940.

This is a PDF file of an article that has undergone enhancements after acceptance, such as the addition of a cover page and metadata, and formatting for readability, but it is not yet the definitive version of record. This version will undergo additional copyediting, typesetting and review before it is published in its final form, but we are providing this version to give early visibility of the article. Please note that, during the production process, errors may be discovered which could affect the content, and all legal disclaimers that apply to the journal pertain.

Credit Author Statement

J.X., C.W. and N.W. contributed equally. J.X., C.W., N.W., L.L., C.C., Z.G. and Y.Z. conceived the project. N.W., C.H., and Y.L. provided the graphdiyne materials. J.X., C.W., N.W., L.M., X.Z. and Y.Y. performed the experiments and analyzed the results. J.X., C.W., N.W., S.Z. and Z.G. wrote the manuscript. The descriptions are agreed by all authors.

Graphdiyne Nanoradioprotector with Efficient Free Radical Scavenging Ability for Mitigating Radiation-induced Gastrointestinal Tract Damage

Jiani Xie[a,b,#], Chengyan Wang[b,c#], Ning Wang[e,#], Shuang Zhu[b], Linqiang Mei[b,c], Xiao Zhang[b], Yuan Yong[g], Lele Li[d], Chunying Chen[d], Changshui Huang[e,*], Zhanjun Gu[b,c*], Yuliang Li[f], Yuliang Zhao[c,d,*]

[a]*College of Pharmacy and Biological Engineering, Chengdu University, Chengdu, 610106, China*

[b]*CAS Key Laboratory for Biomedical Effects of Nanomaterials and Nanosafety, Institute of High Energy Physics, Chinese Academy of Sciences, Beijing, 100049, China*

[c]*Center of Materials Science and Optoelectronics Engineering, College of Materials Science and Optoelectronic Technology, University of Chinese Academy of Sciences, Beijing 100049, China*

[d]*CAS Center for Excellence in Nanoscience, National Center for Nanoscience and Technology of China, Chinese Academy of Sciences, Beijing, 100190, China*

[e]*Qingdao Institute of Bioenergy and Bioprocess Technology, Chinese Academy of Sciences, Qingdao, 266101, China*

[f]*Institute of Chemistry, Chinese Academy of Sciences, Beijing, 100190, China*

[g]*College of Chemistry and Environment Protection Engineering, Southwest Minzu University, Chengdu 610041, China*

 # These authors contributed equally to this work.

*Corresponding authors: zjgu@ihep.ac.cn, huangcs@qibebt.ac.cn,

zhaoyl@nanoctr.cn.

KEYWORDS: graphdiyne, nanoradioprotector, free radical scavenging, oral activity,

gastrointestinal tract

ABSTRACT

X-ray irradiation-induced toxicity to gastrointestinal tract become a significant clinical problem when using radiotherapy for treating abdominal tumors neighbored to gastrointestinal tissue, which not only often prevents these tumors from receiving a definitive therapeutic dose but also causes a series of gastrointestinal diseases, such as anorexia, abdominal pain, diarrhea and hematochezia. And thus it seriously reduces the therapeutic outcome and life quality of patients. Therefore, the development of gastrointestinal radioprotectors is essential. However, the commercial gastrointestinal radioprotectors in clinical are still rare. In view of this, we prepared bovine serum albumin (BSA) modified graphdiyne (GDY) nanoparticles (GDY-BSA NPs) and for the first time studied its gastrointestinal radioprotection ability. The unique advantages of GDY nanomaterial, including high free radical scavenging ability, good chemical stability in gastric acid condition, relatively longer residence time in gastrointestinal tract and good biosafety under oral administration, provide the favorable prerequisites for it to be used as the gastrointestinal radioprotector. In vitro experimental results indicated that the GDY-BSA NPs powerfully reduced DNA damage and improved viability of the irradiated gastrointestinal cells. In vivo results showed that the GDY-BSA NPs significantly decrease radiation-induced diarrhea, weight loss, and gastrointestinal tissue pathological damage of mice. Furthermore, we also deeply studied the gastrointestinal radioprotective mechanism of GDY-BSA NPs, which indicated that the GDY-BSA NPs effectively inhibited reactive oxygen species (ROS)-induced apoptosis signal pathway, and thus reduced gastrointestinal cell

apoptosis. Our work for the first time employed BSA-GDY NPs to mitigating radiation-induced gastrointestinal tract damage, which not only promotes the exploration of new gastrointestinal tract radioprotectors, but also is the good guidance for the treatment of gastrointestinal diseases by nano-drug.

1. Introduction

Radiation therapy is one of the mainstream treatment methods in clinic.[1] The therapeutic index of radiotherapy relies on two major factors, tumor inhibition and normal tissue tolerance.[2] Despite high doses of radiation may be able to maximize tumor cell killing, radiation dose escalation is restricted by its toxicity to neighboring healthy tissues. This limitation applies particularly to the gastrointestinal tract such as small intestine, which is the second most radiation sensitive organ in the body.[3] For example, pelvic and abdominal cancers, such as prostate and pancreatic adenocarcinoma, are very difficult to be eradicated by radiation alone because these tumors need large doses of high energy radiation for control, but are usually adjacent to the radiation sensitive structures of the gastrointestinal tract.[3-5] Therefore, X-ray irradiation induced toxicity to gastrointestinal tract becomes a serious clinical problem, which not only limits the radiation therapeutic dose but also causes a series of gastrointestinal diseases such as radio-induced enteritis or other adverse reactions to patients after radiotherapy. These side-effects make patients anorexia, vomiting, nausea, abdominal pain, rectal bleeding and so on, greatly reducing their life quality.[6-9] Thus, the development of novel radioprotectors to shield gastrointestinal tract from radiation-induced damage could not only ameliorate life quality of patients by mitigating the aforementioned side effects, but also make the therapeutic window increase to enable dose escalation so as to meet more effective tumor cell killing.

Currently, there are no effective drugs for radiation-induced gastrointestinal damage in clinic.[3, 4, 10] Although amifostine has been approved by the Food and

Drug Administration (FDA) to be used in clinical for radioprotection, it is mainly employed to reduce the side-effects in patients undergoing radiotherapy for head and neck cancer.[11, 12] Meanwhile, as a typical molecular drug, amifostine has some inherent defects: (i) its half-life is so short that the elimination of amifostine from body is too fast, which leads to the low bioavailability.[11, 13] (ii) Similar to lots of small molecular drugs, it is not effective when used by oral administration but often requires intravenous injection.[14, 15] However, oral administration is the best manner of drug for gastrointestinal tract treatment because it is the most convenient and quick way for the drug to arrive in gastrointestinal tract. Also, the drug that can stay in gastrointestinal tract for a relatively long time so as to be fully utilized is also desired. Amifostine thus does not meet such requirements for gastrointestinal tract radioprotection. Therefore, these facts motivate us to exploit new types of radioprotectors for gastrointestinal radioprotection. Recently, researchers discovered that some nano-drugs possess free radical scavenging activity, which is even higher than molecular radical scavengers. For instance, it is reported that the antioxidant activity of C_{60} fullerene is hundreds of times more than vitamin C.[16] Moreover, unlike the molecular drug, the nano-drugs have much longer systemic circulation in the body and good stability in various physiological environments.[17] Based on these properties, researchers have spared a lot of efforts for the exploration of nanoradioprotectors, mainly involving carbon-based nanoradioprotectors[18-24], transition-metal dichalcogenide nanoradioprotectors[25-28], cerium-based nanoradioprotectors[29, 30] and noble metal nanoradioprotectors[31, 32]. However,

6

the studies of using the nanoradioprotector for gastrointestinal tract radioprotection are still rare or not deeply studied yet.

In view of these facts, we developed the graphdiyne nanoparticles (GDY NPs) as the new nanoradioprotector for efficient gastrointestinal radioprotection (**Scheme 1**). The unique physical and chemical properties endow the GDY NP a good candidate as an efficient gastrointestinal radioprotector. Firstly, The GDY has strong delocalized π-conjugated structure as well as highly reactive diacetylenic linkages, which makes it possess highly efficient and extensive radical scavenging activity.[22, 33-36] Secondly, The GDY NPs exhibit good chemical stability in the strong acid condition of gastric juice, and thus, it can be injected by oral administration. Thirdly, because of its nanoscale size, the GDY nano-drug can stay in gastrointestinal tract for a relatively long time. These features make GDY NPs not only efficiently scavenge reactive oxygen species (ROS) under oral way and thus protect the gastrointestinal tract during the radiotherapy, but also have low toxicity because it could be efficiently excreted after the treatment. Based on the facts, we prepared bovine serum albumin (BSA) modified GDY NPs (GDY-BSA NPs) and studied its radioprotection behavior for gastrointestinal system. The cell viability assay, clonogenic assay and DNA damage assay indicated that the BSA-GDY NPs can effectively reduce the radiation-induced gastrointestinal cell damage, which is achieved by inhibiting the ROS-induced apoptotic signaling pathway, involving scavenging radiation-induced ROS, reducing ROS-caused mitochondria damage, inhibiting the release of cytochrome c from mitochondria to cytoplasm and decreasing the activation of caspase 3. We further

7

showed that BSA-GDY NPs could powerfully relieve the body weight loss, radiation-caused diarrhea as well as gastrointestinal tissue pathological damage of mice. Consequently, the BSA-GDY NPs are well candidates to be developed as the gastrointestinal radioprotector. Our work for the first time highlights the potential of BSA-GDY NPs for gastrointestinal radioprotectors and encourages further in-depth investigation of nanoscale radioprotectors for gastrointestinal tract disease treatments.

2. Materials and methods

2.1. Materials

BSA was obtained from Beijing Biodee Biotechnology Co. Ltd. Amifostine was purchased from Shanghai yuanye Bio-Technology Co., Ltd. 1,1-Diphenyl-2-picrylhydrazyl radical (DPPH), potassium persulphate and $FeSO_4$ were supplied by Alfa Aesar. 2,2'-Azinobis(3-ethylbenzthiazoline-6-sulfonate) (ABTS) was provided by Sigma-Aldrich. Nicotinamide adenine dinucleotide (NADH) and nitroblue tetrazolium chloride (NBT) were purchased from Beyotime Biotechnology. Phenazine methosulfate (PMS) was provided by Shanghai Aladdin Bio-Chem Technology Co., Ltd. TMB was obtained from Tokyo Chemical Industry Co., Ltd. Cyanine dye was purchased from Innochem (Beijing) Technology Co., Ltd. Rat small intestinal crypt epithelial cells (IEC-6 cells) were obtained from Shanghai fuxiang Biotechnology Co., Ltd. Phosphate buffered saline (PBS) was supplied by HyClone company. Dulbecco's modified eagle medium (DMEM) and fetal bovine serum (FBS) were purchased from Gibco company. Paraformaldehyde was purchased

from Boster Biological Technology Co., Ltd. Triton X-100 were provided by Amresco. Anti-rabbit IgG (H + L), PhosphoHistone H2A.X (Ser139) (20E3) Rabbit mAb and MitoTracker® Deep Red FM were supplied by Cell Signaling Technology. CCK-8 and Giemsa's Stain Kit were obtained from Solarbio Life Sciences. Hoechst 33342, ROS Assay Kit, GSH and GSSG Assay Kit, Mitochondrial Membrane Potential Assay Kit (JC-1), Cytochrome c Mouse Antibody, Alexa Fluor 488-labeled Goat Anti-Mouse IgG (H+L) and Caspase 3 Activity Assay Kit were provided by Beyotime Biotechnology.

2.2 Characterzation.

Transmission electron microscope (TEM, JEM2100Plus) was employed to characterize the size of the product. Dynamic light scattering (DLS, NanoBrook Omni) was used to perform the hydrodynamic size of the product. UV-vis spectrophotometer (Hitachi U-3900) was taken to record the absorption spectra of sample. In vivo fluorescence imaging system (IVIS Spectrum, PerkinElmer) was chose to investigate the biodistribution of GDY-BSA NPs in mice under oral administration. Microplate reader (Thermo Fisher MK3) was used to detect the absorbance of sample. Confocal laser scanning microscope (Nikon A1) and fluorescence inverted microscope (Olympus IX73) was applied for the imaging of cells or tissues. Flow cytometer (BD Accuri C6, USA) was adopted to analyze fluorescent probe signal in the cells.

2.3. The preparation of GDY NPs

The GDY NPs were prepared according to our previous report[22]. In brief, 50 mg of as-synthetized GDY powder was ground by the agate pestle and agate mortar for 10 min. Then, it was dispersed in 50 mL of ultrapure water and subsequently treated with tip-probe ultrasonication under ice-bath to obtain GDY NPs (8 h, 400 W).

2.4. The preparation of GDY-BSA NPs

The GDY-BSA NPs were prepared through a simple physical adsorption method. Briefly, BSA was mixed with GDY NPs with the mass ratio 1:1. Then, this mixture was stirred on the magnetic stirrer (12 h, room temperature) to obtain GDY-BSA NPs.

2.5. The chemical stability of GDY NPs in strong acid

Firstly, GDY NPs solution (□ pH=1) was prepared with 0.1 M hydrochloric acid, and GDY NPs solution (□ pH=7) was prepared with ultrapure water. Then, the absorption spectrum of GDY NPs solution with pH=1 and pH=7 were measured on UV-vis spectrophotometer in 0, 1, 3, 5, 24, 48 and 72 h, respectively.

2.6. DPPH free radical scavenging assay

The DPPH free radical possesses characteristic absorption at 517 nm. And this characteristic absorption value will decrease when DPPH free radical reacts with the radical scavenger. On the basis of the reduced absorption value, we can calculate the free radical scavenging ratio. The experimental procedures are as follows: DPPH was

dissolved in ethanol to obtain 100 µM of DPPH solution. GDY-BSA NPs and amifostine aqueous solutions were set as various concentrations with 10, 20, 30, 50 and 100 µg/mL. Then, the DPPH solution was added into GDY-BSA NPs and amifostine solutions (volume ratio = 1:1) respectively, and these mixtures were reacted in dark for 30 min. After that, the absorbance value in 517 nm of each solution was detected on UV-vis spectrophotometer. The DPPH scavenging ratio (%) was calculated as follow: DPPH scavenging ratio = $((A_{control} - A_{sample})/A_{control}) \times 100$. The $A_{control}$ is the absorbance value of a standard sample without any radical scavengers, and the A_{sample} is absorbance value of un-scavenged DPPH after reacted with radical scavenger.

2.7. ABTS free radical scavenging assay

The ABTS free radical possesses characteristic absorption at 734 nm. And this characteristic absorption value will decrease when ABTS free radical reacts with the radical scavenger. On the basis of the reduced absorption value, we can calculate the ABTS free radical scavenging ratio. The experimental procedures are as follows: First, the ABTS stock solution (7 mM) was mixed with potassium persulphate (2.45 mM), and this mixture was placed in the dark for 16 h to generate ABTS free radical. After that, the as-prepared ABTS radical solution was diluted with PBS until the absorbance value of 734 nm was around 0.7 so as to obtain ABTS radical working solution. Then, GDY-BSA NPs and amifostine aqueous solutions were set as various concentrations with 10, 20, 30, 50 and 100 µg/mL. Afterward, the ABTS radical working solution

11

was added into GDY-BSA NPs and amifostine solutions (volume ratio = 1:1) respectively, and these mixtures were reacted in dark for 10 min. After that, the absorbance value in 734 nm of each solution was detected on UV-vis spectrophotometer. The ABTS free radical scavenging ratio (%) was calculated as follow: ABTS free radical scavenging ratio = $((A_{control} - A_{sample})/A_{control}) \times 100$. The $A_{control}$ is the absorbance value of a standard sample without any radical scavengers, and the A_{sample} is absorbance value of un-scavenged ABTS free radical after reacted with radical scavenger.

2.8. Superoxide radical ($O_2^-\bullet$) scavenging assay

The $O_2^-\bullet$ generated from NADH/PMS system can react with NBT to produce blue chromagen formazan, where the blue chromagen formazan has a characteristic absorption value at 560 nm. If the $O_2^-\bullet$ is consumed by radical scavenger, the yield of blue chromagen formazan will decrease, which indicates as the decrease of characteristic absorption value. The experimental procedures are as follows: it first needed to prepare 1 mM NADH, 0.25 mM NBT and 15 μM PMS. Then, 500 μg/mL GDY-BSA NPs and 500 μg/mL amifostine were prepared as the sample to be tested. Next, 200 μL of PBS, 100 μL of NADH, 100 μL of NBT and 100 μL of the sample was mixed in a quartz cuvette with the final concentrations of NADH (200 μM), NBT (50 μM) and sample (100 μg/mL). Finally, 100 μL of PMS was added into the mixture to initiate the reaction, and the absorbance value in 560 nm of reaction system was real-time monitored for 10 min on UV-vis spectrophotometer.

12

2.9. Hydroxyl radical (•OH) scavenging assay

The •OH generated from the classical Fenton reaction (H_2O_2 and Fe^{2+}) can react the TMB to produce oxTMB, where the oxTMB has a characteristic absorption value at 652 nm. If the •OH is consumed by radical scavenger, the yield of oxTMB will decrease, which indicates the decrease of characteristic absorption value. The experimental procedures are as follows: it first needed to prepare 1 mM TMB (solvent: DMSO), 4 mM $FeSO_4$ (solvent: HAc-NaAc buffer, pH 4.0) and 40 mM H_2O_2 (solvent: ultrapure water). Then, 400 µg/mL GDY-BSA NPs and 400 µg/mL amifostine was prepared as sample to be tested. Next, 150 μL of TMB, 150 μL of H_2O_2, 150 μL of sample and 150 μL of $FeSO_4$ were mixed in a quartz cuvette with the final concentrations of TMB (250 μM), H_2O_2 (10 mM), sample (100 µg/mL) and $FeSO_4$ (1 mM). Subsequently, the mixture was placed in dark for 5 min. Finally, the absorbance value in 652 nm of reaction system was measured on UV-vis spectrophotometer.

2.10. The residence time assay of GDY-BSA NPs in gastrointestinal tract after oral administration

Fluorescence imaging technology was used to monitor the residence time of GDY-BSA NPs in gastrointestinal tract. Firstly, we modified cyanine fluorescent dye onto GDY-BSA NPs to obtain GDY-BSA/cyanine NPs. Briefly, 1 mg of cyanine dye was mixed with 5 mL GDY-BSA NPs (1 mg/mL). And this mixture was stirred on the

13

magnetic stirrer under room temperature for 24 h. Subsequently, the excess cyanine dye was eliminated by centrifugation. After that, the resulted GDY-BSA/cyanine NPs were washed with water and re-suspended for further use. Then, the mice, which fasted the day before the experiment, were orally injected with GDY-BSA/cyanine NPs (12.5 mg/kg). And at the time point of 15 min, 1.5 h, 4 h, 9 h and 24 h, mice were sacrificed and the corresponding organs of heart, liver, spleen, lung, kidney, stomach, small intestine, cecum and colon were collected for fluorescence imaging.

2.11. In vivo biosafety assay of GDY-BSA NPs.

12 healthy BALB/c male mice were divided into 2 groups (each group contains 6 mice): (i) control, (ii) GDY-BSA NPs (oral). The GDY-BSA NPs (12.5mg/kg) were orally injected to the mice of (ii) groups. All the mice were sacrificed at 13th day. The blood samples were obtained via removing the eyeball of mice. 100 µL of blood was stored in vacuum anticoagulant tube (potassium EDTA) for blood routine examinations. The rest of blood samples were kept in 4 °C for 4 h and subsequently centrifuged in refrigerated centrifuge (3500 r, 15 min) to collect blood plasma samples for blood biochemistry assay. In addition, the important organs (including liver, spleen, heart, lung and kidney) were fixed in 4% of formaldehyde, processed into paraffins and stained by H&E, where the as-prepared tissue slices were imaged on fluorescence inverted microscope for pathological analysis.

2.12. The maximum tolerable dose exploration

14

healthy BALB/c mice were divided into 4 groups (each group contains 3 mice): (i) control, (ii) GDY-BSA NPs (oral, 12.5 mg/kg), (iii) GDY-BSA NPs (oral, 50 mg/kg), (iv) GDY-BSA NPs (oral, 100 mg/kg). The GDY-BSA NPs were orally injected to the mice of (ii)-(iv) groups with corresponding dose. After that, the body weights were monitored every other day. And the survival percentages were observed during the experimental period. All the mice were sacrificed after 3 weeks. The blood samples were obtained via removing the eyeball of mice. 100 µL of blood was stored in vacuum anticoagulant tube (potassium EDTA) for blood routine examinations.

2.13. The cytotoxicity of GDY-BSA NPs to IEC-6 cells

The CCK-8 assay was used to detect the cytotoxicity of GDY-BSA NPs to IEC-6 cells. In detail, the IEC-6 cells were planted into 96-well culture plates (8×10^3 per well) and grown in DMEM medium containing 10% of FBS (37 °C, 5% CO_2). After 24 h, the IEC-6 cells were treated with a series of concentrations of GDY-BSA NPs (0, 5, 10, 20, 30, 40, 50, 60, 70, 80, 90 and 100 µg/mL). After another 24 h, the IEC-6 cells were carefully washed with PBS, and co-incubated with 100 µL DMEM medium containing 10% CCK-8 for 1 h (37 °C, 5% CO_2). Eventually, the 96-well plates were centrifuged on the conventional centrifuge (2000 r, 10 min), and the microplate reader was used to measure the absorbance value of supernatants at 450 nm.

2.14. Cellular uptake detection

15

The IEC-6 cells were planted into 24-well culture plates (5×10^4 per well) and grown in DMEM medium containing 10% of FBS (37 °C, 5% CO_2). After 24 h, the IEC-6 cells were treated with GDY-BSA NPs (0 and 50 µg/mL). After another 24 h, the IEC-6 cells were washed by PBS and fixed with paraformaldehyde for 20 min. Next, the cell nuclei were stained by Hoechst 33342. Finally, the cells were imaged under the fluorescence inverted microscope with dark-field accessories.

2.15. The radiation protection activity of GDY-BSA NPs to IEC-6 cells

The CCK-8 assay that detects the cell viability was used to detect the radiation protection activity of GDY-BSA NPs to IEC-6 cells. In detail, the IEC-6 cells were planted into 96-well culture plates (8×10^3 per well) and grown in DMEM medium containing 10% of FBS (37 °C, 5% CO_2). After 24 h, the IEC-6 cells were treated with GDY-BSA NPs (0 and 10 µg/mL). After another 24 h, the IEC-6 cells were irradiated by X-ray tube (AMPTEK Inc.) for 0, 1, 2.5, 5, and 10 min (Voltage: 50 KV, Current: 75 µA), respectively. 24 h after treatment, the IEC-6 cells were carefully washed with PBS, and co-incubated with 100 µL DMEM medium containing 10% CCK-8 for 1 h (37 °C, 5% CO_2). Eventually, the 96-well plates were centrifuged on the conventional centrifuge (2000 r, 10 min), and the microplate reader was used to measure the absorbance value of supernatants at 450 nm.

2.16. Clonogenic assay

16

The clonogenic assay can reflect the survival fraction of cells. In detail, the IEC-6 cells were planted into 6-well culture plates (1×10^3 per well) and grown in DMEM medium containing 10% of FBS (37 °C, 5% CO_2). After 24 h, the IEC-6 cells were treated with GDY-BSA NPs (0 and 10 µg/mL). After another 24 h, the IEC-6 cells were irradiated by X-ray tube for 0 and 30 s (Voltage: 50 KV, Current: 75 µA), respectively. After 4 days, the IEC-6 cells were carefully washed with PBS and treated by Giemsa's stain kit. Finally, the clones were counted in each group and plotted with the survival fraction.

2.17. γ-H2AX staining assay

γ-H2AX staining assay is able to show the DNA damage of cells. In detail, the IEC-6 cells were planted into 24-well culture plates (3×10^4 per well) and grown in DMEM medium containing 10% of FBS (37 °C, 5% CO_2). After 24 h, the IEC-6 cells were treated with GDY-BSA NPs (0 and 10 µg/mL). After another 24 h, the IEC-6 cells were irradiated by X-ray tube for 0 and 10 min (Voltage: 50 KV, Current: 75 µA), respectively. After 3 h, the IEC-6 cells were fixed with 4% paraformaldehyde (10 min). Then, the IEC-6 cells were permeated by 0.2% Triton X-100 (10 min) and treated with the blocking buffer (1 h). Next, the IEC-6 cells were co-incubated with the PhosphoHistone H2A.X (Ser139) (20E3) Rabbit mAb antibody in 4 °C overnight. Afterward, the IEC-6 cells were co-incubated with anti-rabbit IgG (H + L) in 37 °C (1 h) and the cell nuclei were stained with Hoechst 33342. Eventually, the fluorescence imaging of the cells was conducted on the confocal laser scanning microscope.

17

2.18. The GSH level detection

The GSH and GSSG assay kit (Beyotime Biotechnology) was adopted to measure the GSH level in IEC-6 cells. The IEC-6 cells were planted into 6-well culture plates (5×10^5 per well) and grown in DMEM medium containing 10% of FBS (37 °C, 5% CO_2). After 24 h, the IEC-6 cells were treated with GDY-BSA NPs (0 and 10 µg/mL). After another 24 h, the IEC-6 cells were irradiated by X-ray tube for 0 and 15 min (Voltage: 50 KV, Current: 75 µA), respectively. After 6 h, the IEC-6 cells were treated with the GSH and GSSG assay kit and detected on the microplate reader.

2.19. Intracellular ROS assay

The cellular ROS level was tested by the ROS assay kit. In detail, the IEC-6 cells were planted into 35 mm confocal dishes and grown in DMEM medium containing 10% of FBS (37 °C, 5% CO_2). After 24 h, the IEC-6 cells were treated with GDY-BSA NPs (0 and 10 µg/mL). After another 24 h, the IEC-6 cells were treated with the mixture of Hoechst 33342 fluorescent and 2',7'-dichlorodihydrofluorescein diacetate (DCFH-DA) probes at 37 °C for 20 min. Then, the IEC-6 cells were washed with PBS and irradiated by X-ray tube for 0 and 10 min (Voltage: 50 KV, Current: 75 µA), respectively. Eventually, the fluorescence images of the cells were conducted on the confocal laser scanning microscope.

2.20. Mitochondrial membrane potential assay

The mitochondrial membrane potential assay kit (JC-1) was employed to detect the change of mitochondrial membrane potential in IEC-6 cells with deferent treatment. In detail, the IEC-6 cells were planted into 6-well culture plates (5×10^5 per well) and grown in DMEM medium containing 10% of FBS (37 °C, 5% CO_2). After 24 h, the IEC-6 cells were treated with GDY-BSA NPs (0 and 10 µg/mL). After another 24 h, the IEC-6 cells were irradiated by X-ray tube for 0 and 15 min (Voltage: 50 KV, Current: 75 µA), respectively. After 3 h, the IEC-6 cells were treated with the mitochondrial membrane potential assay kit (JC-1). Finally, the cells were detected on flow cytometer.

2.21. The cytochrome c release assay

The co-location assay of mitochondria and cytochrome c can observe the release of cytochrome c from mitochondria. In detail, the IEC-6 cells were planted into 24-well culture plates (3×10^4 per well) and grown in DMEM medium containing 10% of FBS (37 °C, 5% CO_2). After another 24 h, the IEC-6 cells were irradiated by X-ray tube for 0 and 10 min (Voltage: 50 KV, Current: 75 µA), respectively. After 3 h, the IEC-6 cells were stained with MitoTracker® Deep Red FM under 37 °C for 30 min. Then, the IEC-6 cells were fixed with cold 100% methanol in the dark for 15 min. Next, the IEC-6 cells were permeated by 0.2% Triton X-100 (10 min) and treated with the blocking buffer (1 h). After that, the IEC-6 cells were incubated with the cytochrome c mouse antibody at room temperature for 3 h. Subsequently, the

19

IEC-6 cells were incubated with Alexa Fluor 488-labeled Goat Anti-Mouse IgG (H+L) for 1 h, and the cell nuclei were stained with Hoechst 33342. Eventually, the confocal laser scanning microscope was used for co-location analysis of mitochondria and cytochrome c.

2.22. The caspase 3 activity detection

The caspase 3 activity assay kit was employed to measure the caspase 3 activity. In detail, the IEC-6 cells were planted into 6-well culture plates (5×10^5 per well) and grown in DMEM medium containing 10% of FBS (37 °C, 5% CO_2). After 24 h, the IEC-6 cells were treated with GDY-BSA NPs (0 and 10 µg/mL). After another 24 h, the IEC-6 cells were irradiated by X-ray tube for 0 and 15 min (Voltage: 50 KV, Current: 75 µA), respectively. After 6 h, the IEC-6 cells were treated with the caspase 3 activity assay kit and detected on the microplate reader.

2.23. The radiation protection activity of GDY-BSA NPs to gastrointestinal tract under oral administration

24 healthy BALB/c male mice were divided into 4 groups (each group contains 6 mice): (i) control, (ii) GDY-BSA NPs (oral), (iii) X-ray, (iv) GDY-BSA NPs (oral) + X-ray. The GDY-BSA NPs (12.5mg/kg) were orally injected to the mice of (ii) and (iv) groups. After that, the mice in (iii) and (iv) group were radiated with X-ray irradiation (5.5 Gy) by the whole-body exposure pattern. The body weights were monitored daily. And the excretion behavior was observed during the experimental

period. All the mice were sacrificed at 13th day, and the corresponding stomach and intestine were collected for pathological examinations. The experimental procedures of pathological examinations were as follows: the stomach and intestine tissues were first fixed in 4% of formaldehyde. Then, these fixed tissues were processed into paraffins and stainning by hematoxylin and eosin (H&E). Finally, the tissue slices were imaged on fluorescence inverted microscope for pathological analysis.

2.24. The survival data monitoring of mice

Healthy BALB/c mice were divided into 3 groups (each group contains 10 mice): (i) control, (ii) X-ray, (iii) GDY-BSA NPs (oral, 12.5 mg/kg) + X-ray. The GDY-BSA NPs were orally injected to the mice of (iii) groups with drug dose 12.5mg/kg. After that, the mice in (ii) and (iii) group were radiated with X-ray irradiation (5.5 Gy) by the whole-body exposure pattern. The survival percentages were monitored over 30 days.

2.25. The minimum effective dose exploration

Healthy BALB/c mice were divided into 5 groups (each group contains 6 mice): (i) control, (ii) X-ray, (iii) GDY-BSA NPs (oral, 0.78125 mg/kg) + X-ray, (iv) GDY-BSA NPs (oral, 3.125 mg/kg) + X-ray, (v) GDY-BSA NPs (oral, 12.5 mg/kg) + X-ray. The GDY-BSA NPs were orally injected to the mice of (iii), (iv) and (v) groups with corresponding drug dose. After that, the mice in (ii), (iii), (iv) and (v) groups were radiated with X-ray irradiation (5.5 Gy) by the whole-body exposure

21

pattern. All the mice were sacrificed at 13th day, and the corresponding stomach and intestine were collected for pathological examinations.

2.26. The survival data monitoring of mice with different drug doses

Healthy BALB/c mice were divided into 5 groups (each group contains 10 mice): (i) control, (ii) X-ray, (iii) GDY-BSA NPs (oral, 0.78125 mg/kg) + X-ray, (iv) GDY-BSA NPs (oral, 3.125 mg/kg) + X-ray, (v) GDY-BSA NPs (oral, 12.5 mg/kg) + X-ray. The GDY-BSA NPs were orally injected to the mice of (iii), (iv) and (v) groups with corresponding drug dose. After that, the mice in (ii), (iii), (iv) and (v) groups were radiated with X-ray irradiation (5.5 Gy) by the whole-body exposure pattern. The survival percentages were monitored over 30 days. Detailed radiation relevant parameters of the animal experiment: The mice were radiated in the afternoon. Irradiator parameters: radiation dose rate: 1.4 Gy/min; radiation dose: 5.5 Gy; irradiation source to sample distance: 44.5 cm; filter: copper 0.3 mm.

2.27. Statistical analysis

All the data are shown as mean ± standard deviation (SD). Student's *t* test were adopted for statistical analysis of the data between two groups, and p-value < 0.05 was considered to be statistically significant. *: $P < 0.05$; **: $P < 0.01$; ***: $P < 0.001$.

3. Results and discussion

3.1. Synthesis and characterization of GDY-BSA NPs

The GDY was synthesized according to the previous report.[22] Raman and IR spectroscopy of the as-prepared GDY were used to analyze its chemical structure. As seen in **Fig. S1**, four peaks at 1385, 1576, 1927, and 2183 cm^{-1} in the Raman spectrum were detected, where the peaks at 1385 and 1576 cm^{-1} symbolized the D and G bands, respectively, and the peaks at 1927 and 2183 cm^{-1} represented the acetylenic linkages. This result agreed well with the previously reported data.[22, 36] **Fig. S2** indicated the IR spectrum of the as-prepared GDY, where the peaks located at 1492 cm^{-1} and 1658 cm^{-1} were assigned to the skeletal vibrations of aromatic ring. And the peaks at 2102 cm^{-1} and 2190 cm^{-1} were attributed to the typical $C\equiv C$ stretching vibration.[16] The GDY NPs were obtained by ultrasonication methods, and then BSA was modified onto GDY NPs through stirring method to get GDY-BSA NPs. These GDY-BSA NPs are designed to be around 30-40 nm in size by regulating the experimental parameters, which not only enable them well disperse in physiological environment but also are beneficial of then staying in gastrointestinal tract for a relatively long time. As shown in **Fig. 1A and B**, according to the transmission electron microscope (TEM) image and dynamic light scattering (DLS) measurement, the mean size of GDY NPs was around 20 nm (TEM), and the hydrodynamic size of GDY NPs was around 26.06 nm (DLS). Moreover, after BSA modification, the hydrodynamic size of GDY-BSA NPs raised to ～39.03 nm (**Fig. 1C**).

3.2. Chemical stability of GDY NPs in gastric acid environment

For gastrointestinal tract bioapplication, oral administration of drug is the most convenient way to reach the gastrointestinal tract. Thus, the chemical stability of drug in gastric acid environment plays a key role for their performance. However, many of the molecular drugs cannot be used by oral way because their chemical structures will be damaged under the strong acid condition of gastric juice (the pH of gastric juice is about 0.9 ∼ 1.8), resulting in the loss of their drug activity. Therefore, we investigated the chemical stability of GDY NPs under various conditions to judge the feasibility of using GDY-BSA NPs as the gastrointestinal tract radioprotector. As illustrated in **Fig. 1D**, the ultraviolet absorption spectrum of GDY NPs under pH=1 and pH=7 were almost completely overlapped, which suggested that there was no chemical change of the GDY NPs under strong acid environment. Meanwhile, we monitored the ultraviolet absorption change of GDY NPs with time at pH=1 and pH=7, it also could be seen that the spectrum had no obvious change with the time increases (**Fig. 1E and Fig. S3**), which further indicated that the GDY NPs could maintain stabilization both in strong acid and neutral environment. Therefore, these results imply that the GDY NPs possess good chemical stability and thus are able to be employed via oral administration route.

3.3. The comparison of radical scavenging activity between GDY-BSA NPs and amifostine

Radical scavenging process is the commonest radioprotective approach. As a

representative example, amifostine is the most widely used radioprotector in clinic that achieves radioprotection via eliminating the radiation-induced toxic free radical.[37, 38] Therefore, we compared the radical scavenging activity of GDY-BSA NPs with amifostine to preliminarily evaluate the potential of GDY-BSA nanoradioprotector in substituting traditional molecular radioprotector. First, we measured the radical scavenging ratios of GDY-BSA NPs and amifostine to two model stable free radicals (DPPH and ABTS). As seen in **Fig. 1F and G**, under the same mass concentration, both the DPPH and ABTS scavenging ratios of GDY-BSA NPs were much greater than that of amifostine, which indicated the higher radical scavenging ability of GDY-BSA NPs. Then, we compared the radical inhibition action of GDY-BSA NPs and amifostine to the $O_2^-\bullet$ and $\bullet OH$ generation, where the $O_2^-\bullet$ and $\bullet OH$ are two kinds of most important physiologically relevant toxic radicals during radiotherapy. **Fig. 1H** presented the effects of GDY-BSA NPs on $O_2^-\bullet$ scavenging. This assay monitored the characteristic absorbance of blue chromagen formazan that generated by the reaction of $O_2^-\bullet$ with NBT, where the lower absorbance represented the stronger $O_2^-\bullet$ scavenging ability. Hence, the GDY-BSA NPs showed much higher $O_2^-\bullet$ scavenging activity than amifostine under the same mass concentration. **Fig. 1I** reflected the $\bullet OH$ scavenging results of GDY-BSA NPs by 3,3',5,5'-tetramethylbenzidine (TMB) chromogenic route, which detected the characteristic absorbance of oxTMB that produced by the reaction of $\bullet OH$ with TMB. Similar to the $O_2^-\bullet$ scavenging results, the GDY-BSA NPs exhibited stronger scavenging activity toward $\bullet OH$ in comparison to amifostine. As a result, all these free

25

radical scavenging assays indicated that the GDY-BSA nanoradioprotector might have the potential to substitute traditional molecular radioprotector.

3.4. The residence time of the GDY-BSA NPs in gastrointestinal tract under Oral Administration

It is well known that the relatively longer residence time of radioprotector plays a key role in fully fulfilling its drug efficacy in gastrointestinal tract. We thus investigated the residence time of GDY-BSA NPs in gastrointestinal tract after oral administration. As shown in **Fig. 2A and Fig. S4**, fluorescence imaging technology was used to monitor the biodistribution of GDY-BSA NPs in gastrointestinal tract with time. Cyanine fluorescent dye was modified onto GDY-BSA NPs to obtain GDY-BSA/cyanine NPs. Before orally taking GDY-BSA/cyanine NPs (control), no fluorescence signals were monitored in all the tested organs, while the fluorescence signals obviously increased in stomach and small intestine after GDY-BSA/cyanine NPs administration at 15 min, representing the gradual accumulation of GDY-BSA NPs in gastrointestinal tissue. After GDY-BSA/cyanine NPs administration at 1.5 h, the signals also remained strong in stomach and small intestine. At 4th hour, the signals began to be monitored in caecum and colon. And at 9th hour, the signals in stomach and small intestine were sharply reduced but still could be detected, while the signals still remained strong in caecum. It was not until 24th hour that the fluorescence signals in the whole gastrointestinal tract were sharply decreased. This result indicated that the GDY-BSA NPs not only could stay in gastrointestinal tract for

a relatively long time for the full utilization of drug, but also were able to gradually excrete from gastrointestinal tract so as not to cause long-term drug accumulation in the body. More interestingly, during the whole detection time period, we did not observe fluorescence signals in the important organs of heart, liver, spleen, lung and kidney. This phenomenon illuminated that the metabolism of GDY-BSA NPs under oral administration is almost carried out in gastrointestinal tract and it hardly spreads to the other important tissues of the body. Therefore, we can preliminarily estimate that the GDY-BSA NPs do not long-termly accumulate in body to cause toxicity and thus possesses a good biosafety under oral administration. Consequently, the GDY-BSA NPs have a relatively long residence time in gastrointestinal tract, which gives GDY-BSA NPs enough time to exert its radioprotective function for gastrointestinal tissue.

3.5. The biosafety of GDY-BSA NPs in vivo under oral administration

Acceptable biosafety of GDY-BSA NPs is the prerequisite for its gastrointestinal tract radioprotection application. Herein, we evaluated the safety of GDY-BSA NPs to mice under oral administration (oral, 12.5 mg/kg). The histopathology examinations, blood routine and blood biochemistry were adopted to serve as the evaluating indicators. As seen in **Fig. 2B-D** and **Fig. S5**, there were no significant difference of the tissue slices, blood routine indicators and blood biochemistry indicators of the mice treated with or without GDY-BSA NPs (oral) in the tested period, which indicated the good biosafety of GDY-BSA NPs in oral administration and thus

satisfies the prerequisite for radioprotection applications. Then, we explored the maximum tolerable dose. As mentioned above, 12.5 mg/kg of GDY-BSA NPs was a safe dose and exhibited good gastrointestinal tract radioprotection efficacy. We further increased the orally dose of GDY-BSA NPs to mice with 50 mg/kg and 100 mg/kg, and compared the safety data of them. And the data is presented in **Fig. S6**. It could be seen that the survival percentage of mice in all group keep 100% after 3 weeks, and there are no significant differences of mice body weights among all group, which indicated the maximum tolerable dose might be greater than 100 mg/kg from such a macro view. In spite of this, we further tested the blood markers, which revealed that when the drug dose up to 50 mg/kg and 100 mg/kg, the blood markers present tiny discrepancy between the healthy mice group (Control) and the group of mice treated with GDY-BSA NPs. Therefore, the maximum tolerable dose of GDY-BSA NPs should be more than 100 mg/kg.

3.6. In vitro radioprotection efficacy of GDY-BSA NPs

Encouraged by the suitability of GDY-BSA NPs in gastrointestinal tract radioprotection application, we next systematically studied its gastrointestinal tract radioprotection ability in vitro and in vivo. It is known that small intestine is particularly sensitive to radiation among all gastrointestinal tract components.[4] Thus, IEC-6 cell, a typical normal small intestinal cell, was used as the cell model to evaluate the radioprotective potential of GDY-BSA NPs to gastrointestinal tract in vitro. Initially, the cytotoxicity of GDY-BSA NPs to IEC-6 cells was measured by the

standard CCK-8 assay so as to determine its safe concentration to use. According to

the experimental result in **Fig. 3A**, after 24h incubation of GDY-BSA NPs with IEC-6

cells, no obvious toxic effect was detected at all the tested concentrations, even at the

GDY-BSA NPs dosage up to 100 μg mL^{-1}. Then, the uptake of GDY-BSA NPs by

IEC-6 cells was tested (**Fig. S7**), The result indicated that GDY-BSA NPs could be

effective uptake by IEC-6 cells, which is the guarantee for GDY-BSA NPs to exert

drug function in intracellular. Next, the ability of GDY-BSA NPs for IEC-6 cell

radioprotection was evaluated by performing CCK-8 assay, clonogenic assay,

γ-H2AX staining assay and GSH level evaluation. As seen in **Fig. 3B**, CCK-8 assay

was employed to test the cell viabilities of IEC-6 cells treated with or without

GDY-BSA NPs under X-ray radiation exposure. The cell viabilities decrease in

GDY-BSA NPs + X-ray group was remarkably less than the X-ray group treated by

X-ray alone, which indicated that the GDY-BSA NPs could effectively relieve the

X-ray radiation-induced cytotoxicity. Then, clonogenic assay, which assesses the

colony-forming ability of cells, was performed. As depicted in **Fig. S8** and **Fig. 3C**,

the clones were counted in each group and following plotted with the survival fraction.

It could be seen that X-ray treatment drastically decreased the cell survival fraction to

49.18±1.54%. However, when treating the irradiated cells with GDY-BSA NPs, the

survival fraction of GDY-BSA NPs + X-ray group was 61.93±1.59%, which is

obviously more than that of X-ray group. This result demonstrated that GDY-BSA

NPs were able to powerfully defend the X-ray caused cell proliferation inhibition.

Furthermore, γ-H2AX staining assay was used to determine the double-stranded DNA

29

breaks (DSBs). From **Fig. 3D**, to the group of X-ray, significant DSBs were detected in the nuclei of IEC-6 cells. However, the DSBs in the group of GDY-BSA NPs + X-ray were sharply decreased compared to the group of X-ray, which indicated that the GDY-BSA NPs could availably shield DNA from X-ray-induced damage. In addition, intracellular GSH level is also an important radio-protective indicator that reflects cellular redox balance. We thus evaluated the cellular GSH level. As seen in **Fig. S9,** the experimental result indicated that the GDY-BSA NPs could protect the GSH descent in IEC-6 cells after X-ray exposure, which is beneficial to maintain intracellular redox balance. Consequently, GDY-BSA NPs exhibit strong radioprotection effect to IEC-6 cells and thus are promising to act as the gastrointestinal tract radioprotector.

3.7. In vitro radioprotective mechanism study of GDY-BSA NPs

The good radioprotection effect of GDY-BSA NPs to gastrointestinal cell promotes us to deeply study its radioprotective mechanism. It is known that the interaction of high energy ionizing radiation with H_2O or molecules in cell can generate ROS to cause cell damage. As human body contain 80% H_2O, the radiation damage mainly originates from the ROS-induced damage.[39, 40] Meanwhile, the apoptosis and necrosis of cells is programmed, which possesses corresponding signal pathway. We thus investigated the relation of GDY-BSA NP with ROS-induced apoptosis signal pathway in IEC-6 cells to deeply understand its gastrointestinal tract radioprotective mechanism. According to the report, the ROS can cause mitochondrial

dysfunction, and then the cytochrome c will be released from mitochondria to help to

activate caspase 3 (an apoptosis related factor), and finally trigger cell apoptosis.[41]

If the GDY-BSA NPs are able to inhibit this process, the cell death will be reduced.

Following this rationale, we conducted the related experiments. We first detected the

ROS scavenging ability of GDY-BSA NPs in IEC-6 cells. DCFH-DA fluorescent

probe was adopted to monitor ROS generation. As shown in **Fig. 4A**, when treated the

IEC-6 cells with X-ray alone, obvious DCF green fluorescence signal was observed,

indicating high levels of ROS generation. However, when treating the irradiated cells

with GDY-BSA NPs, the fluorescence signal was sharply reduced. In addition,

ignorable signal was observed in the group of control or GDY-BSA NPs-treated alone.

These results indicated that GDY-BSA NPs have powerful ROS scavenging ability.

Then, we measured the mitochondrial membrane potential (MMP) of the IEC-6 cells

with different treatment. In a typical respiration, the energy is produced and stored in

the inner membrane of mitochondria. This process will cause the asymmetric

distribution of protons and other ions on both sides of the mitochondrial inner

membrane, and thus result in the form of MMP.[42] It has been verified that ROS can

cause mitochondrial membrane damage to initiate the cell apoptosis, which presents

as the depolarization of MMP.[43, 44] As seen in **Fig. 4B**, the decrease of red/green

ratio represents the decrease of MMP. After treating the IEC-6 cells with X-ray alone,

the red/green ratio was sharply reduced to $29.07 \pm 5.43\%$ compared to that of control

group ($53.64 \pm 10.44\%$), symbolizing the X-ray-caused mitochondrial dysfunction.

Whereas the red/green ratio in GDY-BSA NPs + X-ray group ($49.29 \pm 3.31\%$) was

comparable to that of control group. This result indicated that the GDY-BSA NPs could effectively relieve radiation-induced mitochondrial dysfunction. We infer that it may attribute to the powerful ROS scavenging ability of GDY-BSA NPs, which consumes the radiation-induced ROS and thus reduces the damage of ROS to mitochondria. Next, according to previous researches, the attack of ROS to mitochondria will increase the mitochondrial membrane permeability and lead to the cytochrome c release from mitochondria into the cytosol.[43] Thus the co-localization analysis between mitochondria and cytochrome c was conducted by confocal laser scanning microscope to monitor the cytochrome c release. As illustrated in **Fig. 4C** and **Fig. S10-11**, the group of control and GDY-BSA NPs alone, displayed the high degree of overlap between mitochondria (red fluorescence) and cytochrome c (green fluorescence) with the Pearson's correlations of 0.872729 and 0.886407, respectively. In contrast, the X-ray alone group presented an obvious separation of red and green fluorescence signal with the Pearson's correlations 0.670679, representing the release of cytochrome c from mitochondria into cytosol. However, it could still maintain a high overlap between mitochondria and cytochrome c in the group of GDY-BSA NPs + X-ray with the Pearson's correlations 0.84863, which demonstrated that the GDY-BSA NPs effectively inhibited the cytochrome c release. Finally, it has been verified that the cytochrome c released into cytosol from mitochondria can interact with cytoplasmic apoptosis activating factor-1 and form a complex, which will help to activate caspase 3 to induce cell apoptosis.[41] Hence, we further measured the caspase 3 activity of the IEC-6 cells with different treatment. From **Fig. 4D**,

32

X-ray-treated cells exhibited remarkable up-regulation of caspase 3 activity into 1.44 $\pm$0.08-fold in comparison to control group. However, when treating the irradiated cells with GDY-BSA NPs, despite the caspase 3 activity of GDY-BSA NPs + X-ray group showed up-regulation into 1.16$\pm$0.05-fold compared to control group, it was still obviously lower than that of X-ray group. This result suggests that the GDY-BSA NPs can inhibit the activation of caspase 3 and thus are beneficial to reduce cell apoptosis. Taken together, the above results indicated that GDY-BSA NPs achieve radioprotection to gastrointestinal cells via inhibiting radiation-related apoptosis signal pathway (**Fig. 4E**).

3.8. In vivo radioprotection efficacy of GDY-BSA NPs to gastrointestinal tract under oral administration

Inspired by satisfying radioprotective effect of the GDY-BSA NPs to gastrointestinal cells in vitro, and its unique superiorities for gastrointestinal tract radioprotection application, we further studied its effectiveness in vivo under oral administration. It is well known that the patients with radiation enteritis usually show symptoms of weight loss, diarrhea, abdominal pain, malabsorption and so on.[9, 45] We thus monitored the body weights, excretion behavior as well as physical appearance of the irradiated mice with GDY-BSA NPs (oral) treatment and analyzed the gastrointestinal tissues pathological changes of the mice to evaluate GDY-BSA NPs' gastrointestinal tract radioprotection ability. The healthy BALB/c male mice were used as research models. 24 mice were divided into 4 groups (6 mice for each

33

group): (i) control, (ii) GDY-BSA NPs (oral, 12.5 mg/kg), (iii) X-ray, (iv) GDY-BSA

NPs (oral, 12.5 mg/kg) + X-ray. All the mice were sacrificed at 13th day when there

was a significant difference of body weights between group of X-ray and GDY-BSA

NPs (oral) + X-ray, and the corresponding stomach and intestine were collected for

pathological analysis. As depicted in **Fig. 5A**, the weight of mice in the X-ray group

presented a persistently decreasing trend. However, when treating the irradiated mice

with GDY-BSA NPs, despite the weight of mice exhibited down-regulation in the first

4 days, it began to recover on the 5th day and showed a persistently increasing trend

in the next days. In the 13th day, the average body weight presented significant

difference between X-ray group (15.86±1.95 g) and GDY-BSA NPs (oral) + X-ray

group (19.47 ± 1.51 g). This result preliminarily suggested the effective

gastrointestinal tract radioprotective activities of GDY-BSA NPs. **Fig. 5B** visually

exhibited the physiology changes of mice after different treatment. There was a

serious diarrhea phenomenon of the mice treated by X-ray alone, which presented as

loose stools. This phenomenon might be ascribed to the X-ray-induced

gastrointestinal dysfunction, which led to the severe diarrhea of the mice. In contrast,

no obvious diarrhea phenomenon was observed to the mice in GDY-BSA NPs (oral) +

X-ray group. This result indirectly verified that the GDY-BSA NPs have the ability for

gastrointestinal tract radioprotection, which could effectively relieve X-ray-induced

gastrointestinal dysfunction so as to reduce the diarrhea. Then, in order to directly

prove the radioprotective effect of GDY-BSA NPs to gastrointestinal tract, we

collected the stomach and intestine tissues for pathological analysis. As shown in **Fig.**

5C, for the stomach tissue in the group of control and GDY-BSA NPs (oral), the structure of adenogastric tissue was clear and well arranged. Meanwhile, the gastric gland of gastric mucosa is neatly arranged, and the gastric pits could be seen clearly. Also, gastric mucosal epithelial cells were columnar without obvious shedding. Therefore, the stomach tissue in these two groups is healthy without structure abnormality or obvious lesion. Conversely, for the stomach tissue of X-ray group, the obvious attenuation and necrosis of gastric wall was found. Meanwhile, there is vacuolization in epidermal cells and hyaline degeneration in lamina propria as well as muscular layer of mucous membrane. And only a few fibroblasts remained. However, for the stomach tissue of GDY-BSA NPs (oral) + X-ray group, although the gastric epithelial cells partially lost, the gastric mucinous gland is normal, the cells in lamina propria of mucosa were arranged orderly and the muscle fiber cells of muscle layer were arranged regularly. Hence, the GDY-BSA NPs could powerfully decrease the radiation-induced stomach damage. Similarly, for the intestinal tissue, the structure of intestinal tissue in control and GDY-BSA NPs (oral) group was clear and well arranged. In detail, their intestinal mucosae were covered by simple ciliated columnar epithelium, and the epithelial cells mixed with a few goblet cells. The mucosa and submucosa protruded to the intestinal cavity and form many policae circulane, where there were irregular leafy or columnar villi on the surface of the policae. Also, Panoth's cells distributed in crypts, whose cytoplasm contained large and round eosinophilic particles. In contrast, the intestinal tissue in X-ray group presented severe total intestinal necrosis, whose intestinal epithelial was necrotic and lost on a large

35

scale, even the nucleus were dissolved and disappeared. However, when treated the irradiated mice with GDY-BSA NPs, the radiation-induced intestinal damage was greatly reduced compared to the X-ray group. In addition, we counted the crypt number, villi number and villi height of the intestine in various treated groups. As seen in **Fig. 5D-F**, the crypt and villi in X-ray treated group could not be counted because the intestinal tissue in X-ray group showed severe total necrosis, which was regarded as 0. However, the crypt number, villi number and villi height of the intestine in GDY-BSA NPs (oral) + X-ray group are 19 ± 2.18/mm, 17.17 ± 1.26/mm and 430 ± 45.82 μm, which are comparable to that of control group with 19 ± 1/mm, 19 ± 1/mm and 500 ± 24.33 μm. Therefore, the GDY-BSA NPs effectively relieved the radiation-induced intestine damage. Next, it is known that the 30-day survival data is basic and very important in evaluation of radioprotective potential. Thus, we also monitored the survival percentage of mice for about a month. From **Fig. S12**, under the whole-body irradiation exposure, it could be seen that when the survival percentage of mice in X-ray group lowered to 30%, the survival percentage of mice in GDY-BSA NPs + X-ray group could still maintain in 90%. And when the mice in X-ray group died all, the survival percentage of mice in GDY-BSA NPs + X-ray group could remain 40%, and it maintains 40% after 30 days. This result indirectly reflected the gastrointestinal tract radioprotection ability of GDY-BSA NPs, where the GDY-BSA NPs effectively reduced the damage of gastrointestinal tract and thus prolonged the lifetime of irradiated mice and even improve the 30-day survival percentage of irradiated mice. As a result, the GDY-BSA NP manifests the ability for

gastrointestinal tract radioprotection and thus has the potential to be developed as the gastrointestinal tract radioprotector.

In addition, in order to find the relationship between drug dose and drug efficacy, we roughly explored the minimum effective dose GDY-BSA NPs for gastrointestinal tract radioprotection. First, we investigated the minimum effective dose. We compared the radioprotective effect of GDY-BSA NPs to stomach and intestinal tissue of mice with different drug concentrations including 0.78125 mg/kg, 3.125 mg/kg, and 12.5 mg/kg (**Fig. S13**). It could be seen that the mice in 12.5 mg/kg GDY-BSA NPs + X-ray group present minimal damage of stomach and intestinal tissue among all irradiated group. The tissue of mice in 3.125 mg/kg GDY-BSA NPs + X-ray group showed moderate injury, whose gastric epithelial cells and intestinal villi lost partially. And the tissue of mice in 0.78125 mg/kg GDY-BSA NPs +X-ray group show serious damage, whose gastric epithelial cells and intestinal villi lost on a large scale, but its injury degree is still less than the group of X-ray alone. Therefore, we roughly estimate the minimum effective dose of GDY-BSA NPs is below 0.78125 mg/kg. Meanwhile, we monitored the 30-day survival data under different drug doses (**Fig. S14**). It showed that when the survival percentage of mice in X-ray group lowered to 10%, the survival percentage of mice in 0.78125 mg/kg GDY-BSA NPs+ X-ray, 3.125 mg/kg GDY-BSA NPs + X-ray and 12.5 mg/kg GDY-BSA NPs+ X-ray group could still maintain in 30%, 40% and 70%, respectively. And the survival percentage of mice in 12.5 mg/kg GDY-BSA NPs + X-ray group remained 40% after 30-day. Although the mice in 0.78125 mg/kg GDY-BSA NPs + X-ray and 3.125 mg/kg

37

GDY-BSA NPs + X-ray group finally died all, they survival time is still longer than the mice in X-ray group. The data further support the results that the minimum effective dose of GDY-BSA NPs should below 0.78125 mg/kg.

4. Conclusion

Overall, in view of the difficult problem that gastrointestinal tract is easy to be destroyed in radiotherapy, we designed and prepared the GDY-BSA NPs for gastrointestinal radiation protection. The as-prepared GDY-BSA NPs possess strong free radical scavenging ability, good biosafety, good chemical stability in gastric acid environment, and relatively long retention time in gastrointestinal tract under oral administration. The cell experimental results showed that GDY-BSA NPs could effectively reduce the radiation-induced DNA damage of IEC-6 cells, relieve the radiation-caused cell growth inhibition and improve the viability of irradiated cells. The animal experimental results showed that GDY-BSA NPs remarkably alleviate the diarrhea, weight loss as well as gastrointestinal tissue pathological damage of irradiated mice. Moreover, we demonstrated that the gastrointestinal radioprotective mechanism of GDY-BSA NPs is to inhibit the ROS-induced apoptosis signal pathway, which consumes the intracellular ROS generated by radiolysis, reduces the ROS-induced mitochondrial membrane damage, inhibits the release of cytochrome c from mitochondria to cytoplasm, decreases the activation of caspase 3, and eventually decreases the cell apoptosis. Therefore, GDY-BSA NPs have a great potential to be developed as the gastrointestinal radioprotector. Our work not only provides a new

38

nanoplatform for the gastrointestinal radioprotection application, but also inspires the development of nano-drug for treatment of gastrointestinal diseases, which is significant to improve life quality of patients.

ASSOCIATED CONTENT

Notes

The authors declare no competing financial interest.

Appendix A. Supplementary data

Supplementary data related to this article can be found at https://

References

[1] G. Song, L. Cheng, Y. Chao, K. Yang, Z. Liu, Emerging nanotechnology and advanced materials for cancer radiation therapy, Adv. Mater. 29 (2017) 1700996.
[2] E. Rannou, A. Francois, A. Toullec, O. Guipaud, V. Buard, G. Tarlet, E. Mintet, C. Jaillet, M.L. Iruela-Arispe, M. Benderitter, J.C. Sabourin, F. Milliat, In vivo evidence for an endothelium-dependent mechanism in radiation-induced normal tissue injury, Sci. Rep. 5 (2015) 15738.
[3] M. de la Cruz Bonilla, K.M. Stemler, C.M. Taniguchi, H. Piwnica-Worms, Stem cell enriched-epithelial spheroid cultures for rapidly assaying small intestinal

radioprotectors and radiosensitizers in vitro, Sci. Rep. 8 (2018) 15410.

[4] M. Li, A. Du, J. Xu, Y. Ma, H. Cao, C. Yang, X.D. Yang, C.G. Xing, M. Chen, W. Zhu, S. Zhang, J. Cao, Neurogenic differentiation factor NeuroD confers protection against radiation-induced intestinal injury in mice, Sci. Rep. 6 (2016) 30180.

[5] M. Hauer-Jensen, J.W. Denham, H.J. Andreyev, Radiation enteropathy—pathogenesis, treatment and prevention, Nat. Rev. Gastro. Hepat. 11 (2014) 470-479.

[6] M.T.W. Teo, D. Sebag-Montefiore, C.F. Donnellan, Prevention and management of radiation-induced late gastrointestinal toxicity, Clin. Oncol. 27 (2015) 656-667.

[7] H.J. Andreyev, A.C. Muls, C. Norton, C. Ralph, L. Watson, C. Shaw, J.O. Lindsay, Guidance: The practical management of the gastrointestinal symptoms of pelvic radiation disease, Frontline Gastroenterol. 6 (2015) 53-72.

[8] K. Dennis, M. Poon, E. Chow, Nausea and vomiting induced by gastrointestinal radiation therapy: current status and future directions, Curr. Opin. Support. Palliat. Care 9 (2015) 182-188.

[9] S. Ali, I. Habib, S. Ali, Pharmacological interventions for the prevention and treatment of radiation colitis, enteritis and proctitis, Cochrane Db. Syst. Rev. (2011).

[10] Q. Hou, L. Liu, Y. Dong, J. Wu, L. Du, H. Dong, D. Li, Effects of Thymoquinone on radiation enteritis in mice, Sci. Rep. 8 (2018) 15122.

[11] L.K. Mell, B. Movsas, Pharmacologic normal tissue protection in clinical radiation oncology: focus on amifostine, Expert Opin. Drug Metab. Toxicol. 4 (2008) 1341-1350.

[12] J.J. Varghese, I.L. Schmale, D. Mickelsen, M.E. Hansen, S.D. Newlands, D.S.W. Benoit, V.A. Korshunov, C.E. Ovitt, Localized delivery of amifostine enhances salivary gland radioprotection, J. Dent. Res. 97 (2018) 1252-1259.

[13] W.J. van der Vijgh, A.E. Korst, Amifostine (Ethyol): pharmacokinetic and pharmacodynamic effects in vivo, Eur. J. Cancer 32A Suppl 4 (1996) S26-30.

[14] G. A, L. Ren, Z. Zhou, D. Lu, S. Wang, Design and evaluation of biodegradable enteric microcapsules of amifostine for oral delivery, Int. J. Pharm. 453 (2013) 441-447.

[15] T.L. Lu, W.G. Sun, W. Zhao, T. Chen, Preparation of amifostine polylactide-co-glycolide microspheres and its irradiation protective to mouse through oral administration, Drug Dev. Ind. Pharm. 37 (2011) 1473-1480.

[16] F. Huang, Z. Zhang, F. Yang, K. Yang, Research progresson physical and chemical property and application of fuilerene[60], Journal of Iiaocheng University(Nat. Sci.) 27 (2014) 32-36.

[17] J. Xie, C. Wang, F. Zhao, Z. Gu, Y. Zhao, Application of multifunctional nanomaterials in radioprotection of healthy tissues, Adv. Healthcare Mater. 7 (2018) e1800421.

[18] Q. Zhao, Y. Li, J. Xu, R. Liu, W. Li, Radioprotection by fullerenols of Stylonychia mytilus exposed to gamma-rays, Int. J. Radiat. Biol. 81 (2005) 169-175.

[19] B. Daroczi, G. Kari, M.F. McAleer, J.C. Wolf, U. Rodeck, A.P. Dicker, In vivo radioprotection by the fullerene nanoparticle DF-1 as assessed in a zebrafish model, Clin. Cancer Res. 12 (2006) 7086-7091.

[20] Y. Qiao, P. Zhang, C. Wang, L. Ma, M. Su, Reducing X-ray induced oxidative damages in fibroblasts with graphene oxide, Nanomaterials (Basel) 4 (2014) 522-534.

[21] J. Xie, Y. Yong, X. Dong, J. Du, Z. Guo, L. Gong, S. Zhu, G. Tian, S. Yu, Z. Gu, Y. Zhao, Therapeutic nanoparticles based on curcumin and bamboo charcoal nanoparticles for chemo-photothermal synergistic treatment of cancer and radioprotection of normal cells, ACS Appl. Mater. Interfaces 9 (2017) 14281-14291.

[22] J. Xie, N. Wang, X. Dong, C. Wang, Z. Du, L. Mei, Y. Yong, C. Huang, Y. Li, Z. Gu, Y. Zhao, Graphdiyne nanoparticles with high free radical scavenging activity for radiation protection, ACS Appl. Mater. Interfaces 11 (2019) 2579-2590.

[23] X. Ren, M. Huo, M. Wang, H. Lin, X. Zhang, J. Yin, Y. Chen, H. Chen, Highly catalytic niobium carbide (MXene) promotes hematopoietic recovery after radiation by free radical scavenging, ACS Nano 13 (2019) 6438-6454.

[24] J. Wang, X. Cui, H. Li, J. Xiao, J. Yang, X. Mu, H. Liu, Y.-M. Sun, X. Xue, C. Liu, X.-D. Zhang, D. Deng, X. Bao, Highly efficient catalytic scavenging of oxygen free radicals with graphene-encapsulated metal nanoshields, Nano Res. 11 (2018) 2821-2835.

[25] X.D. Zhang, J. Zhang, J. Wang, J. Yang, J. Chen, X. Shen, J. Deng, D. Deng, W. Long, Y.M. Sun, C. Liu, M. Li, Highly catalytic nanodots with renal clearance for radiation protection, ACS Nano 10 (2016) 4511-4519.

[26] J. Du, Z. Gu, L. Yan, Y. Yong, X. Yi, X. Zhang, J. Liu, R. Wu, C. Ge, C. Chen, Y. Zhao, Poly(Vinylpyrollidone)- and selenocysteine-modified Bi2Se3 nanoparticles enhance radiotherapy efficacy in tumors and promote radioprotection in normal tissues, Adv. Mater. 29 (2017) 1701268.

[27] H. Liu, J. Wang, Y. Jing, J. Yang, X. Bai, X. Mu, F. Xu, X. Xue, L. Liu, Y.-M. Sun, Q. Liu, H. Dai, C. Liu, X.-D. Zhang, Renal clearable luminescent WSe2 for radioprotection of nontargeted tissues during radiotherapy, Part. Part. Syst. Charact. 34 (2017) 1700035.

[28] X.D. Zhang, Y. Jing, S. Song, J. Yang, J.Y. Wang, X. Xue, Y. Min, G. Park, X. Shen, Y.M. Sun, U. Jeong, Catalytic topological insulator Bi2Se3 nanoparticles for invivo protection against ionizing radiation, Nanomedicine 13 (2017) 1597-1605.

[29] R.W. Tarnuzzer, J. Colon, S. Patil, S. Seal, Vacancy engineered ceria nanostructures for protection from radiation-induced cellular damage, Nano Lett. 5 (2005) 2573-2577.

[30] A.L. Popov, S.I. Zaichkina, N.R. Popova, O.M. Rozanova, S.P. Romanchenko, O.S. Ivanova, A.A. Smirnov, E.V. Mironova, I.I. Selezneva, V.K. Ivanov, Radioprotective effects of ultra-small citrate-stabilized cerium oxide nanoparticles in vitro and in vivo, RSC Adv. 6 (2016) 106141-106149.

[31] D.K. Chandrasekharan, P.K. Khanna, C.K.K. Nair, Cellular radioprotecting potential of glyzyrrhizic acid, silver nanoparticle and their complex, Mutat. Res. 723 (2011) 51-57.

[32] J.Y. Wang, X. Mu, Y. Li, F. Xu, W. Long, J. Yang, P. Bian, J. Chen, L. Ouyang, H. Liu, Y. Jing, J. Wang, L. Liu, H. Dai, Y. Sun, C. Liu, X.D. Zhang, Hollow PtPdRh nanocubes with enhanced catalytic activities for in vivo clearance of radiation-induced ROS via surface-mediated bond breaking, Small 14 (2018)

e1703736.

[33] J. Liu, C. Chen, Y. Zhao, Progress and prospects of graphdiyne-based materials in biomedical applications, Adv. Mater. 31 (2019) e1804386.

[34] H. Yu, Y. Xue, Y. Li, Graphdiyne and its assembly architectures: synthesis, functionalization, and applications, Adv. Mater. 31 (2019) e1803101.

[35] C. Huang, Y. Li, N. Wang, Y. Xue, Z. Zuo, H. Liu, Y. Li, Progress in research into 2D graphdiyne-based materials, Chem. Rev. 118 (2018) 7744-7803.

[36] G. Li, Y. Li, H. Liu, Y. Guo, Y. Li, D. Zhu, Architecture of graphdiyne nanoscale films, Chem. Commun. 46 (2010) 3256-3258.

[37] G.J. Peters, W.J.F. van der Vijgh, Protection of normal tissues from the cytotoxic effects of chemotherapy and radiation by amifostine (WR-2721): preclinical aspects, Eur. J. Cancer 31 (1995) S1-S7.

[38] T.K. Lee, R.M. Johnke, R.R. Allison, K.F. O'Brien, L.J. Dobbs, Jr., Radioprotective potential of ginseng, Mutagenesis 20 (2005) 237-243.

[39] C.K.K. Nair, D.K. Parida, T. Nomura, Radioprotectors in radiotherapy, J. Radiat. Res. 42 (2001) 21-37.

[40] J. Xie, L. Gong, S. Zhu, Y. Yong, Z. Gu, Y. Zhao, Emerging strategies of nanomaterial-mediated tumor radiosensitization, Adv. Mater. 31 (2019) e1802244.

[41] K. Ni, G. Lan, S.S. Veroneau, X. Duan, Y. Song, W. Lin, Nanoscale metal-organic frameworks for mitochondria-targeted radiotherapy-radiodynamic therapy, Nat. Commun. 9 (2018) 4321.

[42] Y. Liu, J.L. Hu, M.G. Li, G.X. Ma, L. Han, Y.Z. Huang, Correlation of mitochondria membrane potential of vascular endothelial cells to hypoxia and angiotesin, Clin. J. Med. Offic. 36 (2008) 485-487.

[43] H. Wang, Y. Chen, N. Zhai, X. Chen, F. Gan, H. Li, K. Huang, Ochratoxin A-induced apoptosis of IPEC-J2 cells through ROS-mediated mitochondrial permeability transition pore opening pathway, J. Agric. Food Chem. 65 (2017) 10630-10637.

[44] H.U. Simon, A. Haj-Yehia, F. Levi-Schaffer, Role of reactive oxygen species (ROS) in apoptosis induction, Apoptosis 5 (2000) 415-418.

[45] D. Yao, L. Zheng, J. Wang, M. Guo, J. Yin, Y. Li, Perioperative alanyl-glutamine-supplemented parenteral nutrition in chronic radiation enteritis patients with surgical intestinal obstruction: a prospective, randomized, controlled study, Nutr. Clin. Pract. 31 (2016) 250-256.
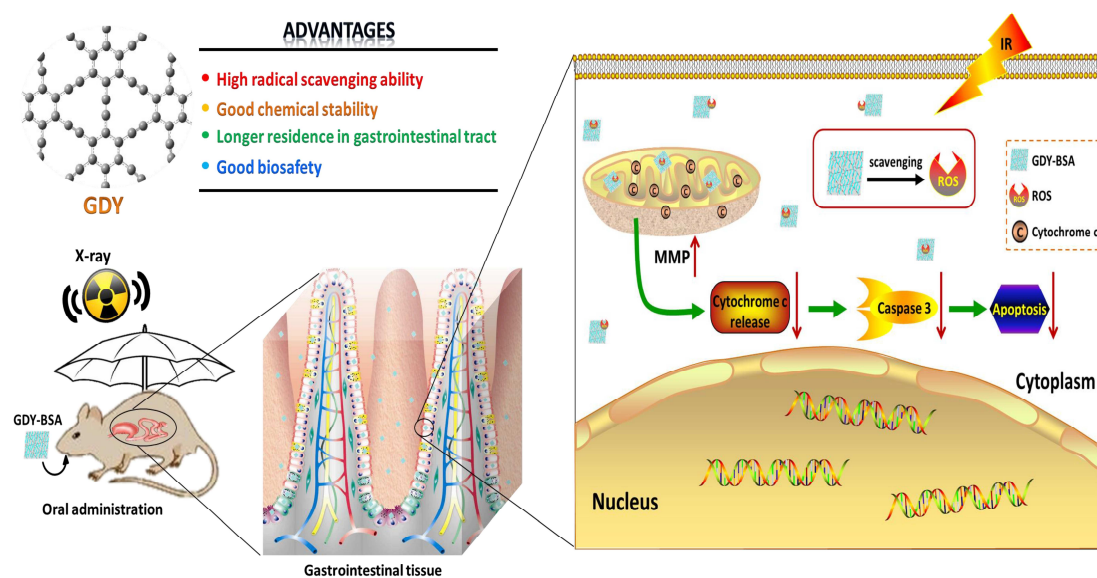
Scheme 1. Schemes of the GDY-BSA NPs for gastrointestinal radioprotection.
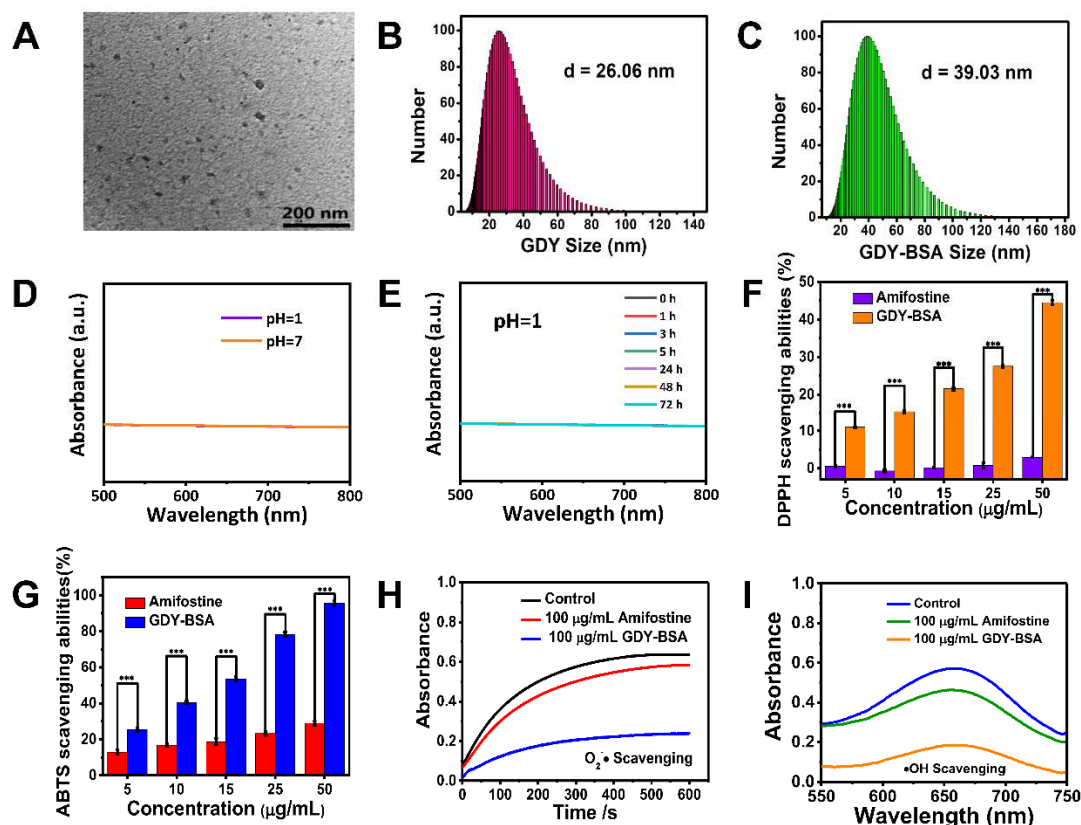
Fig. 1. (A) The TEM image of as-prepared GDY NPs. (B) The hydrodynamic size of GDY NPs. (C) The hydrodynamic size of GDY-BSA NPs. (D) UV−vis−NIR absorption spectra of GDY NPs under pH=1 and pH=7, respectively. (E) UV−vis−NIR absorption spectra of GDY NPs at different time points under pH=1. (F) The comparison of DPPH radical scavenging ratios between amifostine and GDY-BSA NPs, respectively. (G) The comparison of ABTS radical scavenging ratios between amifostine and GDY-BSA NPs, respectively. (H) The comparison of $O_2^-\cdot$ scavenging ability between amifostine and GDY-BSA NPs, respectively. (I) The comparison of $\cdot OH$ scavenging ability between amifostine and GDY-BSA NPs, respectively. (*: $P < 0.05$; **: $P < 0.01$; ***: $P < 0.001$.)

44
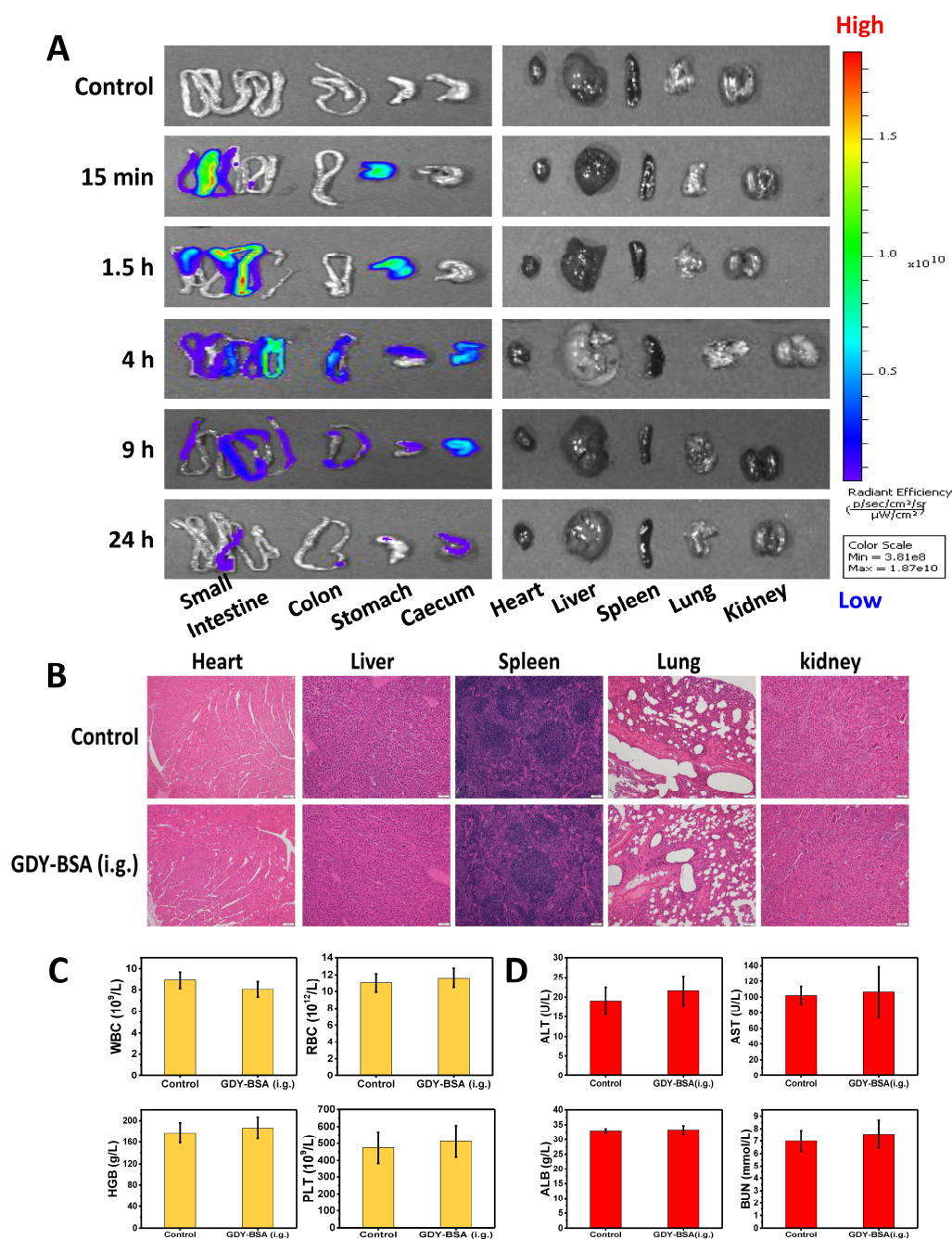
Fig. 2. (A) In vivo fluorescence imaging of various organs in mice after oral administration of GDY-BSA/cyanine NPs at different time points. (B) The histopathology analysis of mice after different treatments. (C) The blood routine examination of mice after different treatments. (D) The blood biochemistry data of mice after different treatments.
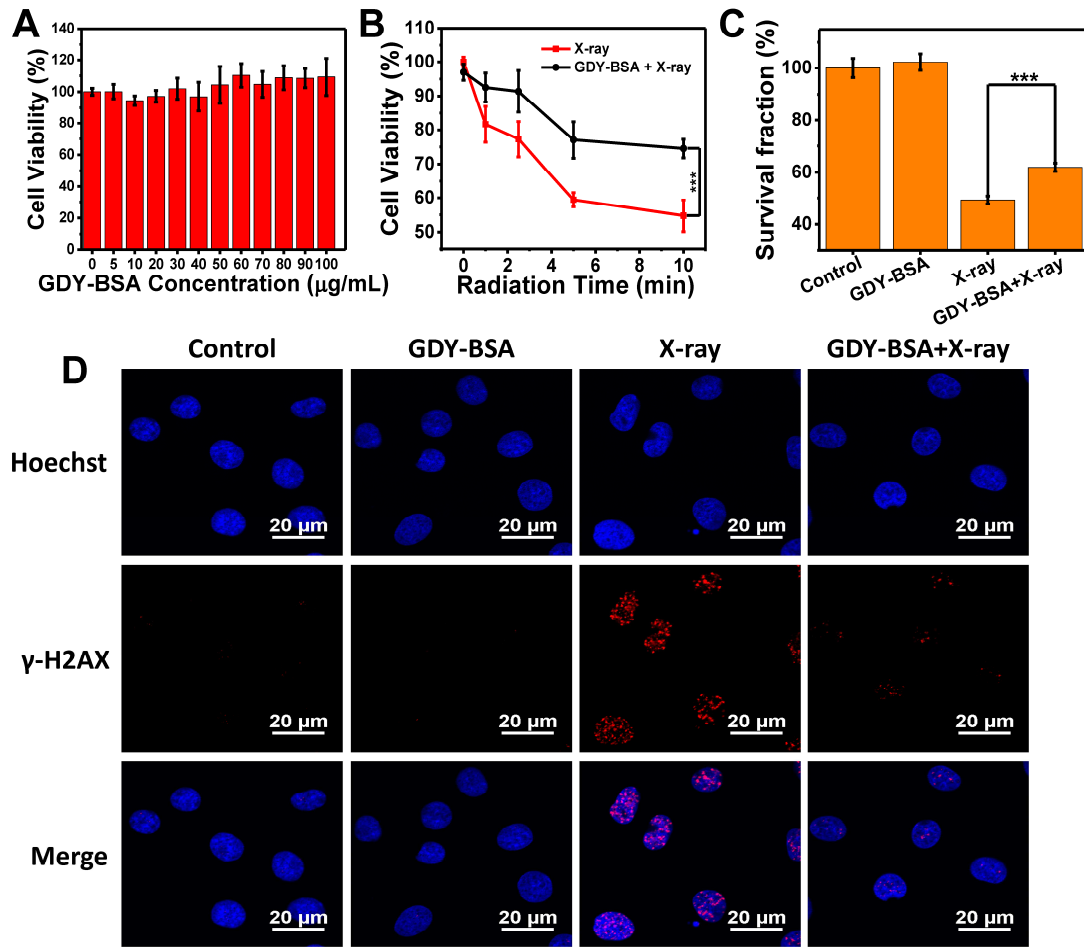
Fig. 3. (A) The cell viability of IEC-6 cells treated by different concentrations of GDY-BSA NPs. (B) Radiation protection of IEC-6 cells by GDY-BSA NPs under different radiation doses. (C) Survival fraction of IEC-6 cells after different treatments in clone assay. (D) DNA double-strand damage in IEC-6 cells after different treatments by γ-H2AX immufluorescence assay. (*: P < 0.05; **: P < 0.01; ***: P < 0.001.)

46
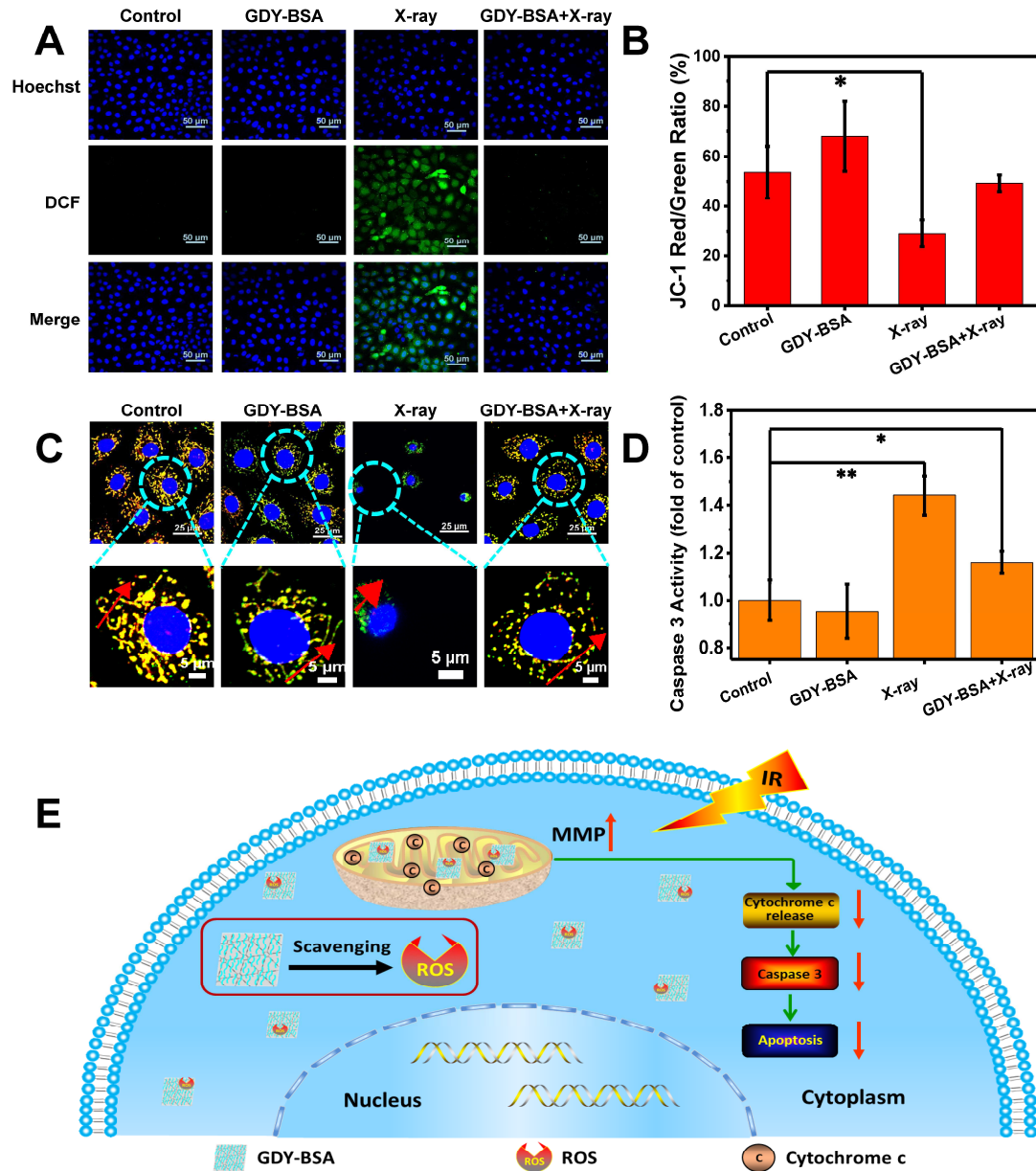
Fig. 4. (A) Fluorescence images about the intracellular ROS generation in IEC-6 cells after different treatments. (B) JC-1 red/green ratio of IEC-6 cells after different treatments. (C) The co-location of cytochrome c and mitochondria in IEC-6 cells after different treatments. (D) Caspase 3 activity of IEC-6 cells after different treatments. (E) The radioprotective mechanism of GDY-BSA NPs in IEC-6 cells. (*: $P < 0.05$; **: $P < 0.01$; ***: $P < 0.001$.)

47
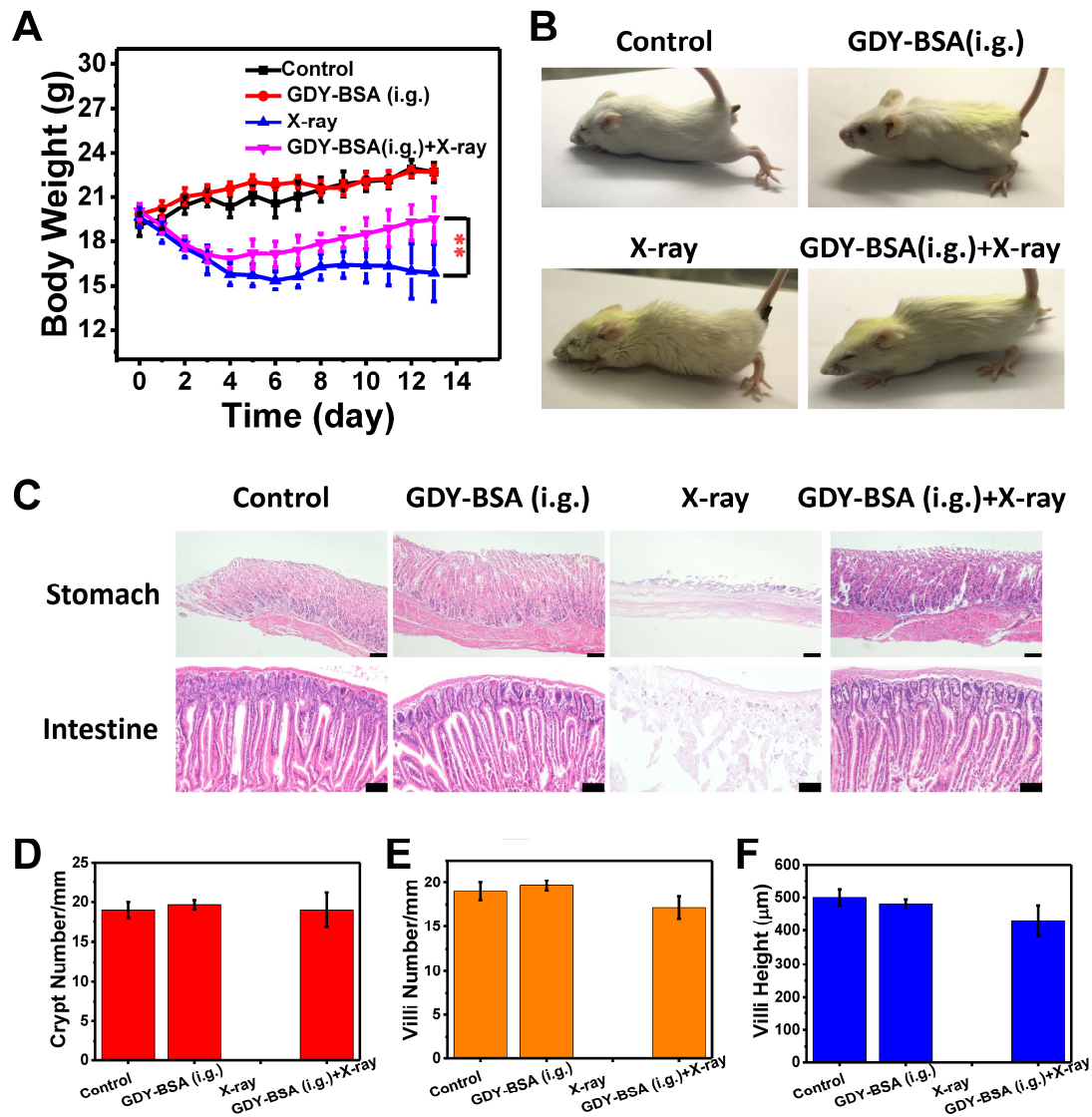
Fig. 5. (A) The body weights change of mice with time after different treatments. (B) The physiology changes of mice after different treatments. (C) Histopathology analysis of mice after different treatments (including stomach and intestine), and the scale bar represent 50 μm. (D, E, F) The crypt number, villi number and villi height analysis in intestine of mice after different treatments, respectively. (*: $P < 0.05$; **: $P < 0.01$; ***: $P < 0.001$.) The oral drug dose of GDY-BSA NPs is 12.5 mg/kg.

48

TOC
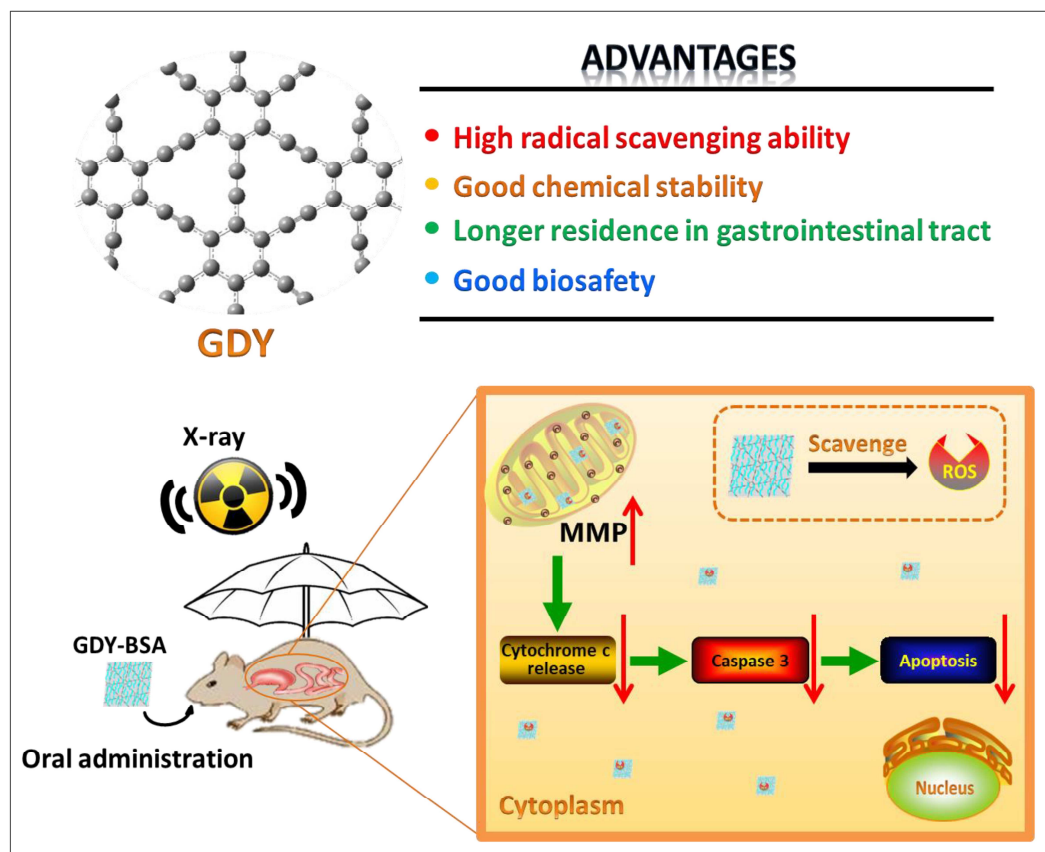
Supporting Information

Graphdiyne Nanoradioprotector with Efficient Free Radical Scavenging Ability for Mitigating Radiation-induced Gastrointestinal Tract Damage

Jiani Xie[a,b,#], Chengyan Wang[b,c,#], Ning Wang[e,#], Shuang Zhu[b], Linqiang Mei[b,c], Xiao Zhang[b], Yuan Yong[g], Lele Li[d], Chunying Chen[d], Changshui Huang[e,*], Zhanjun Gu[b,c,*], Yuliang Li[f], Yuliang Zhao[c,d,*]
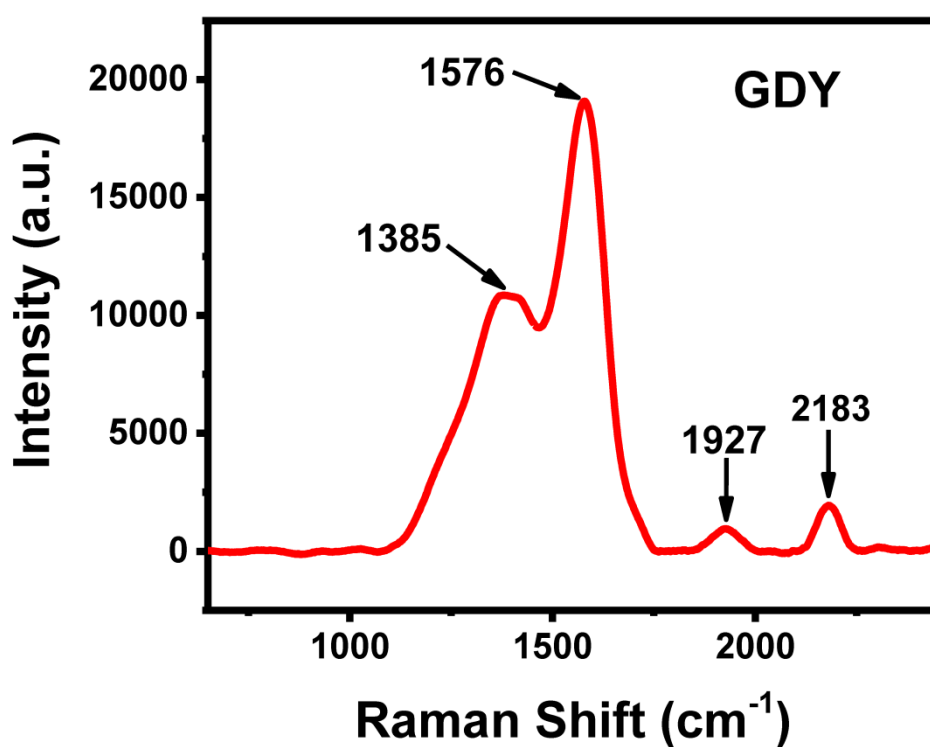
Fig. S1. Raman absorption spectra of GDY.
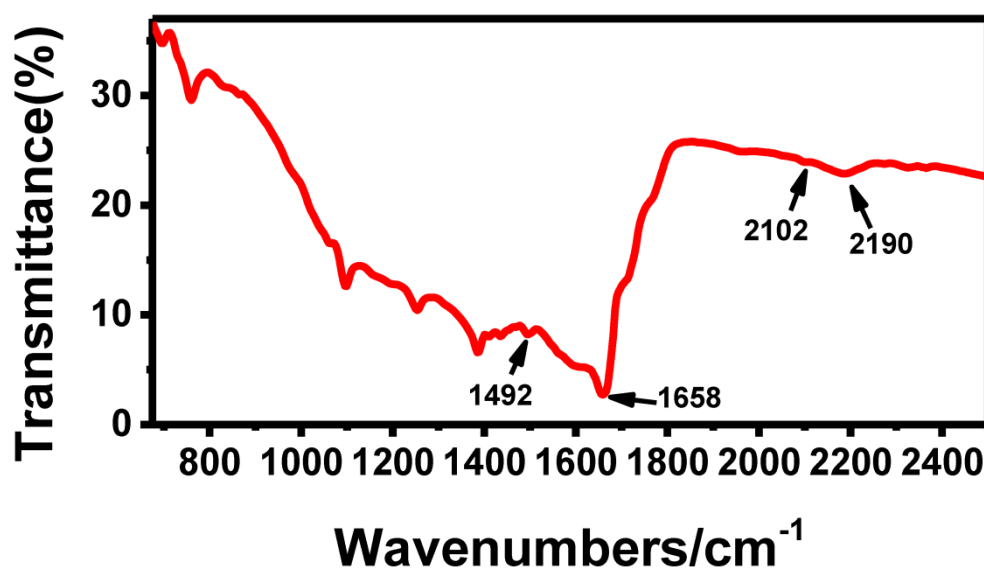
Fig. S2. IR absorption spectra of GDY.
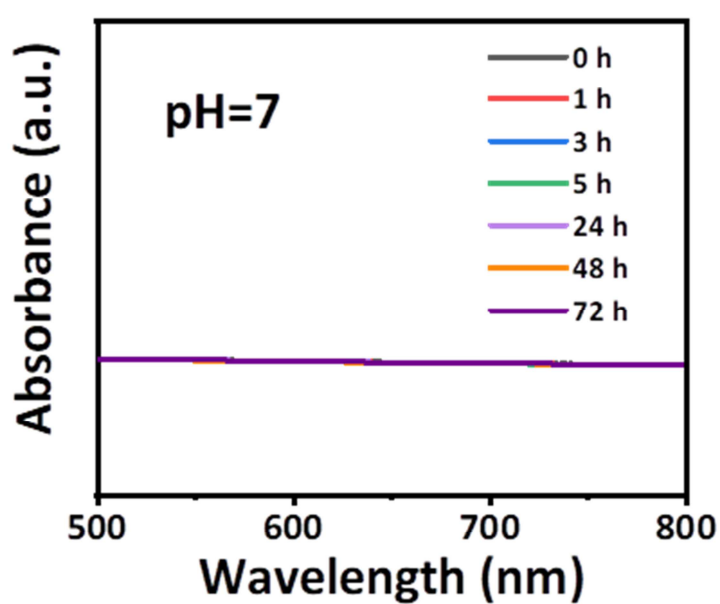
Fig. S3. UV−vis−NIR absorption spectra of GDY NPs at different time points under

pH=7.

52
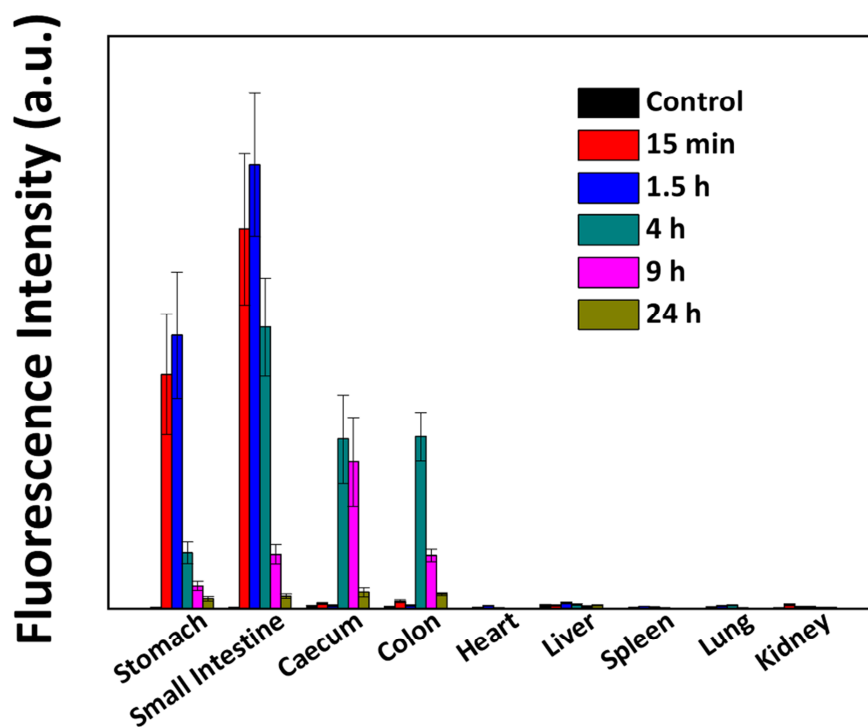
Fig. S4 The fluorescence intensity analysis in mice after oral administration of

GDY-BSA/cyanine NPs at different time points.
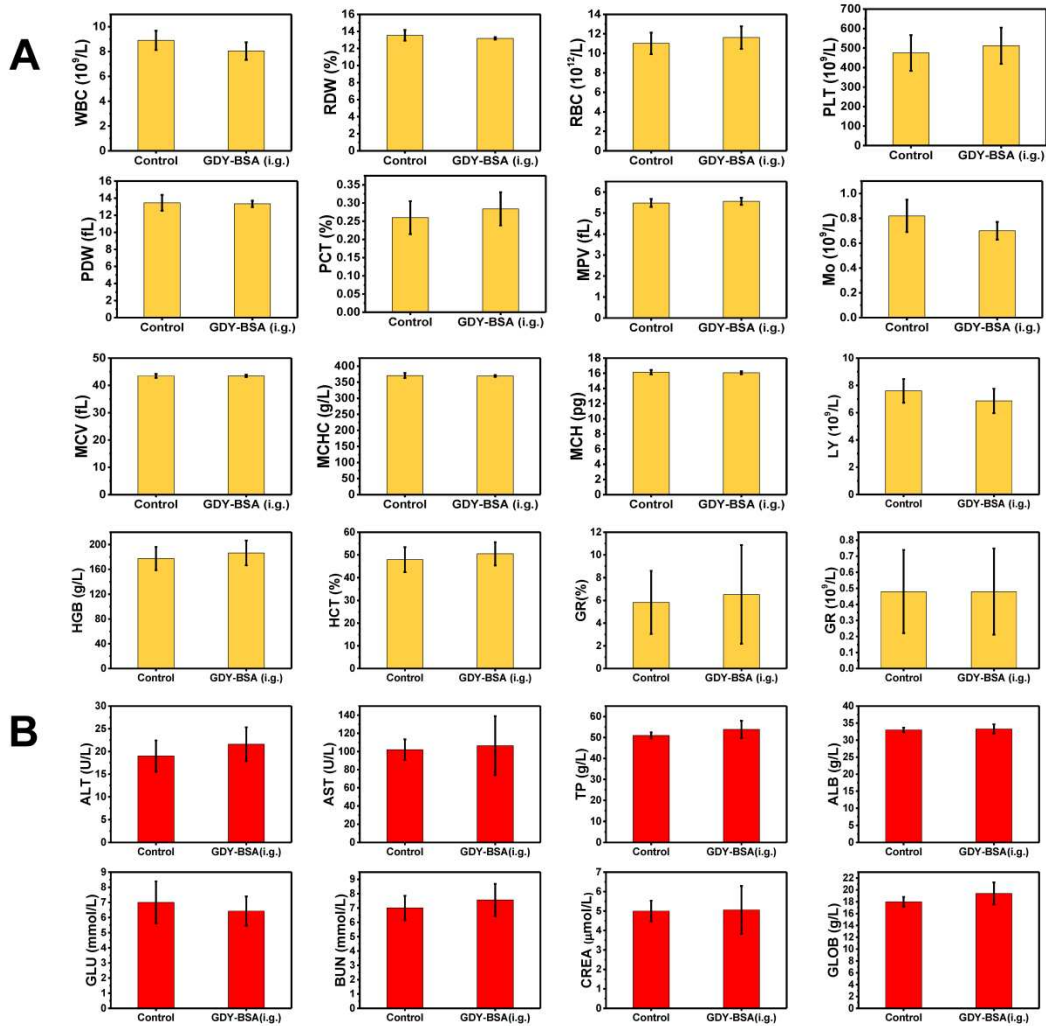
Fig. S5. (A) The blood routine examination of mice after different treatments. (B) The

blood biochemistry data of mice after different treatments.
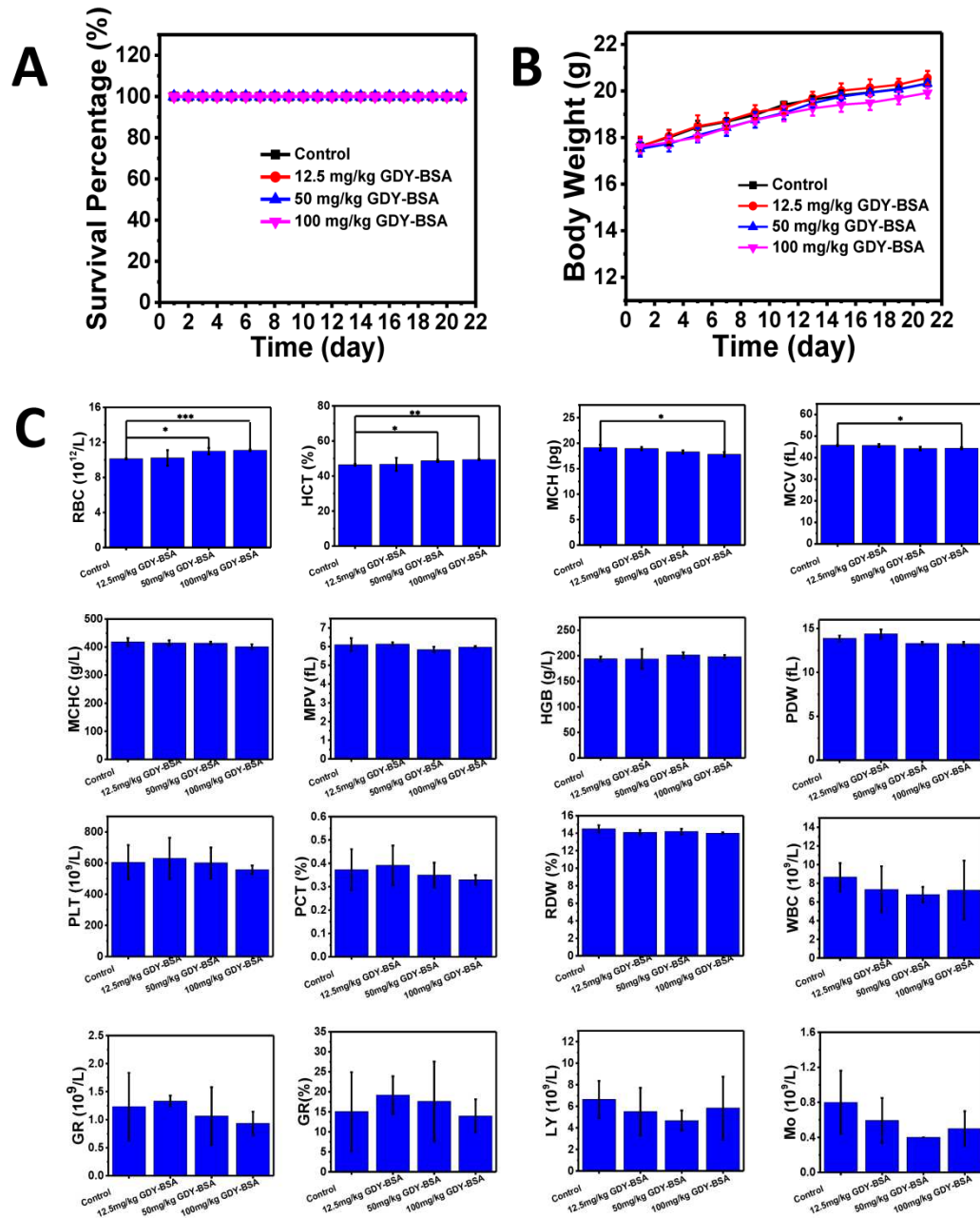
Fig. S6 The maximum tolerable dose exploration. (A) The survival percentage of mice with time after different treatments. (B) The body weights of mice with time after different treatments. (C) The blood markers data of mice after different treatments (*: P < 0.05; **: P < 0.01; ***: P < 0.001.).

54
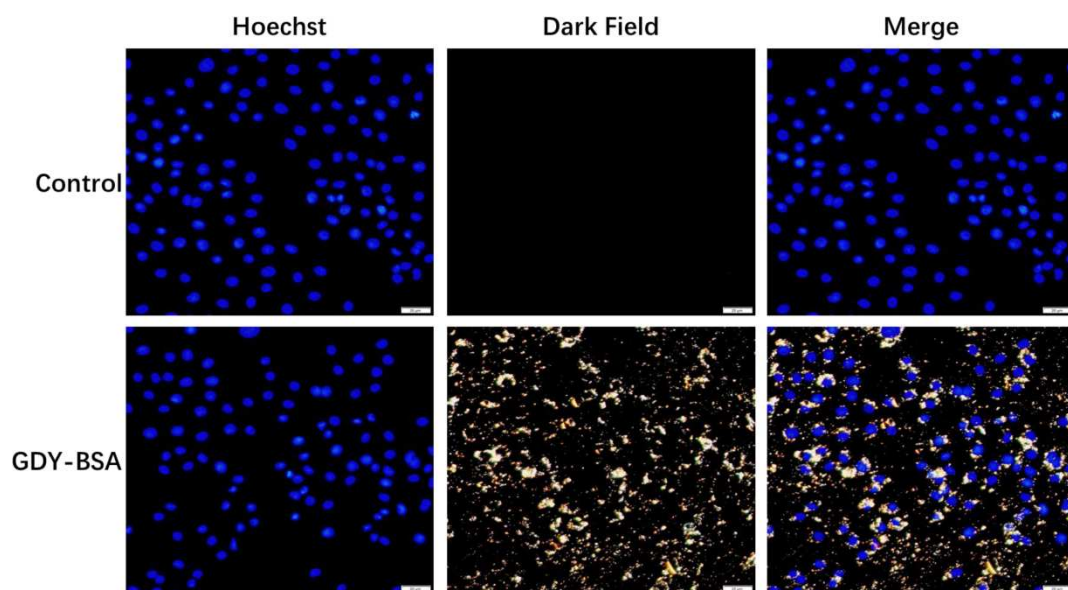
Fig. S7. The uptake of GDY-BSA NPs by IEC-6 cells. This result indicated that our

GDY-BSA NPs could be effective uptake by IEC-6 cells.
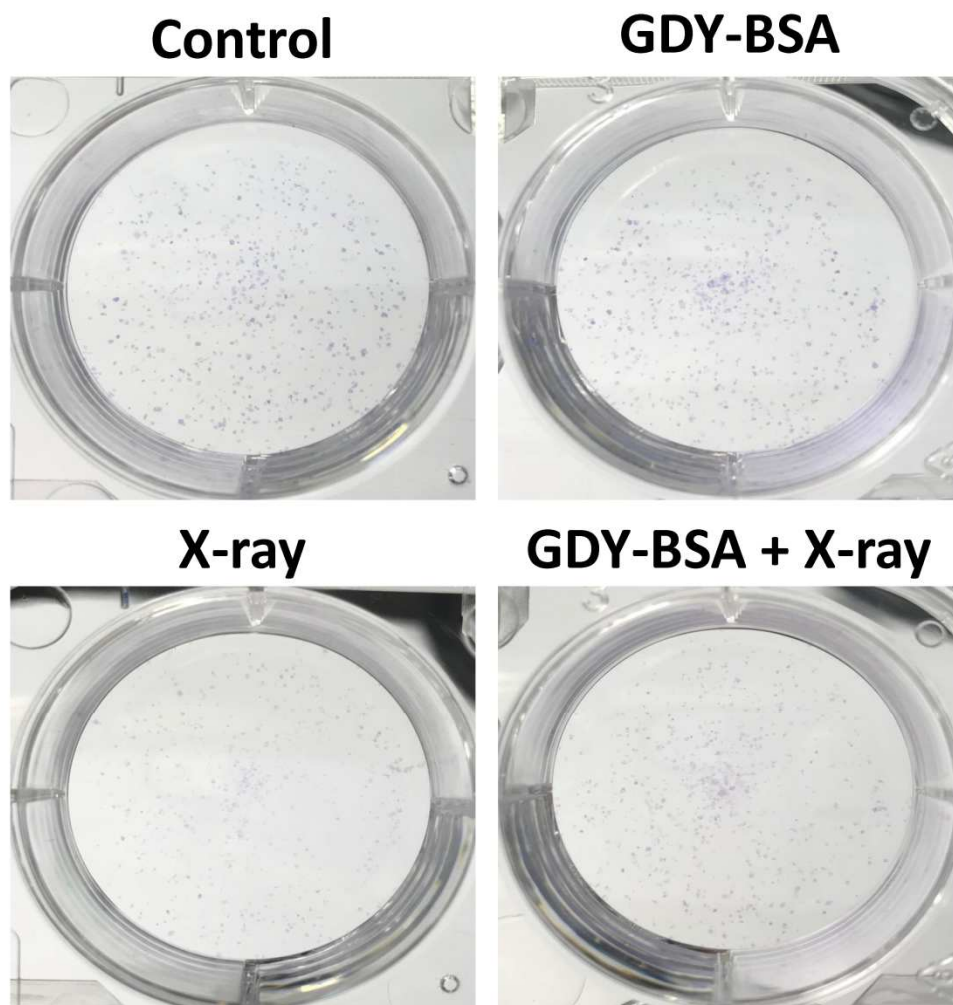
Group	Survival fraction (%)
Control	100±3.67
GDY-BSA	102.29±3.18
X-ray	49.18±1.54
GDY-BSA + X-ray	61.93±1.59

Fig. S8. Colony of IEC-6 cells after different treatments.
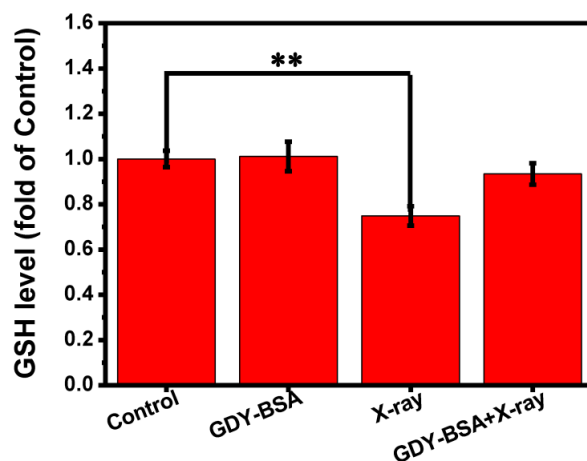
Fig. S9. The evaluation of cellular glutathione (GSH) level in IEC-6 cells after different treatments. GSH level is important for cellular redox balance. This result indicated that the GDY-BSA NPs could protect the GSH descent in IEC-6 cells after X-ray exposure (*: $P < 0.05$; **: $P < 0.01$; ***: $P < 0.001$.).
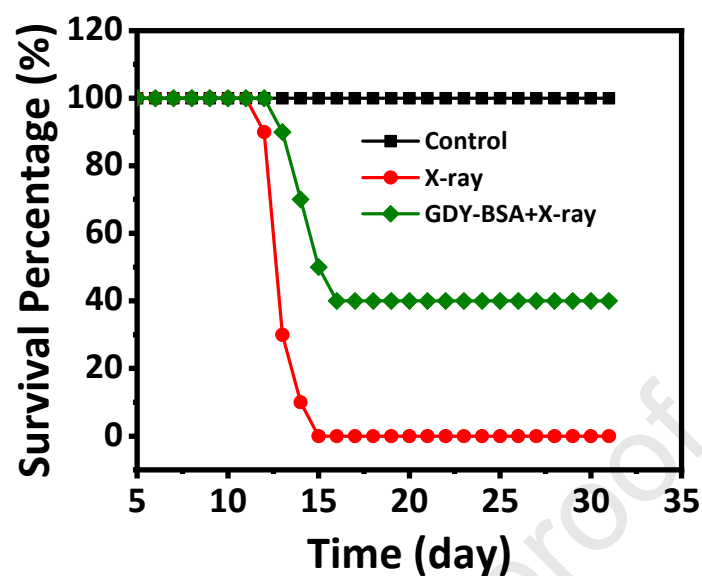
Group	Pearson's correlation
Control	0.872729
GDY-BSA	0.886407
X-ray	0.670679
GDY-BSA + X-ray	0.84863
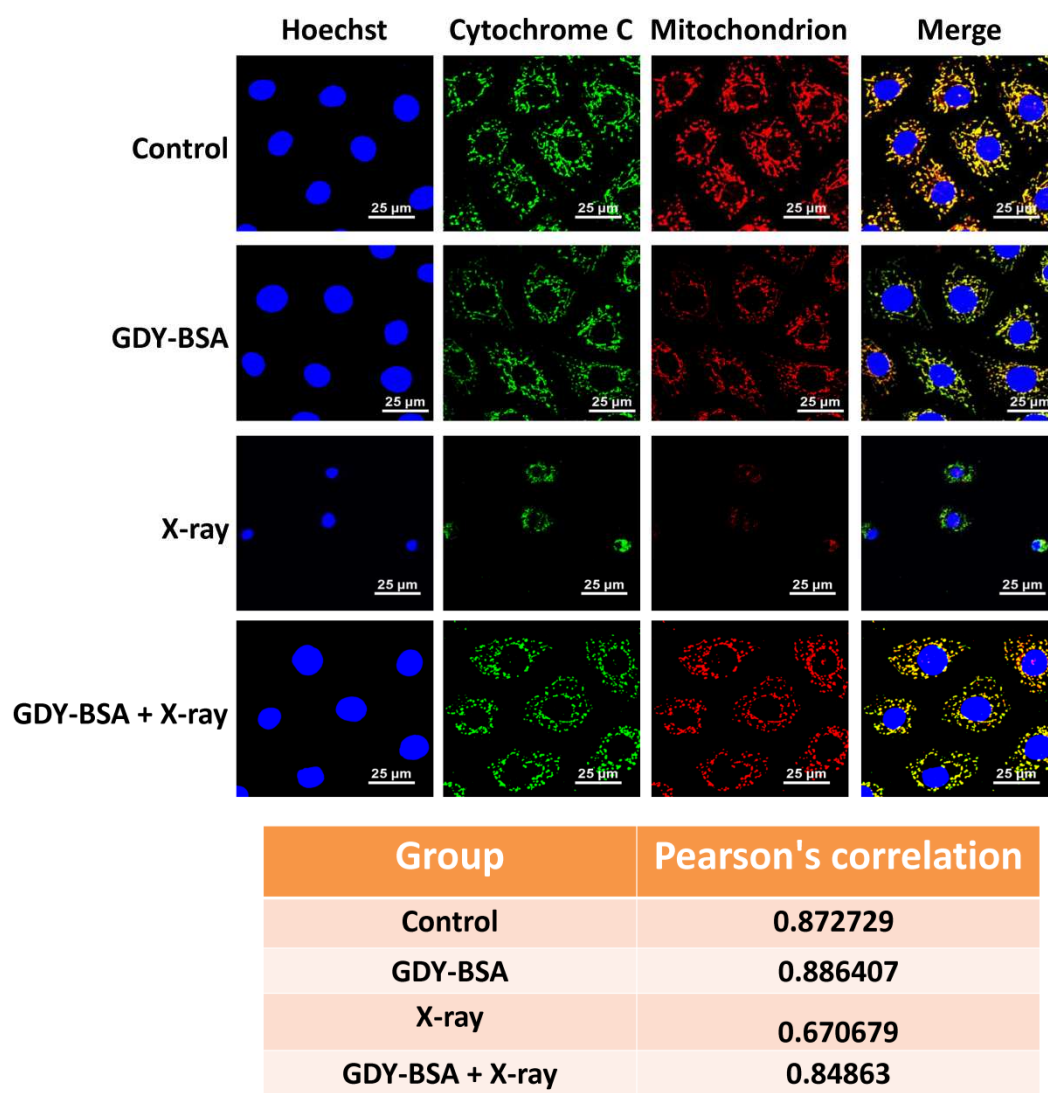
Fig. S10. The co-location imaging of cytochrome c and mitochondria in IEC-6 cells after different treatments.
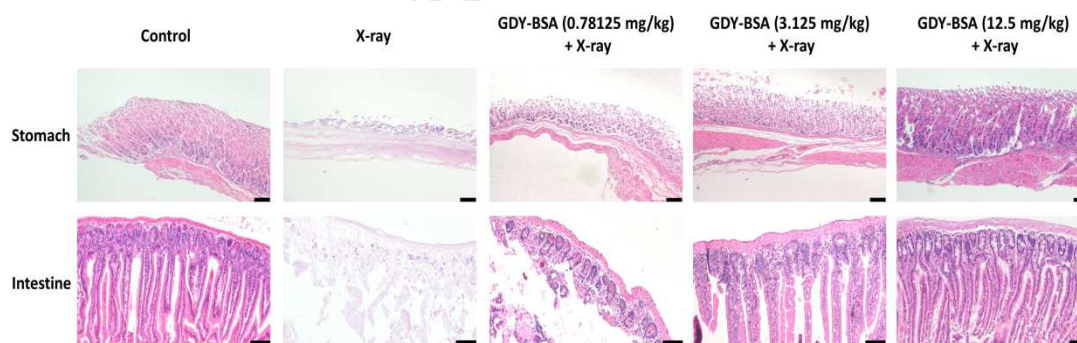
58
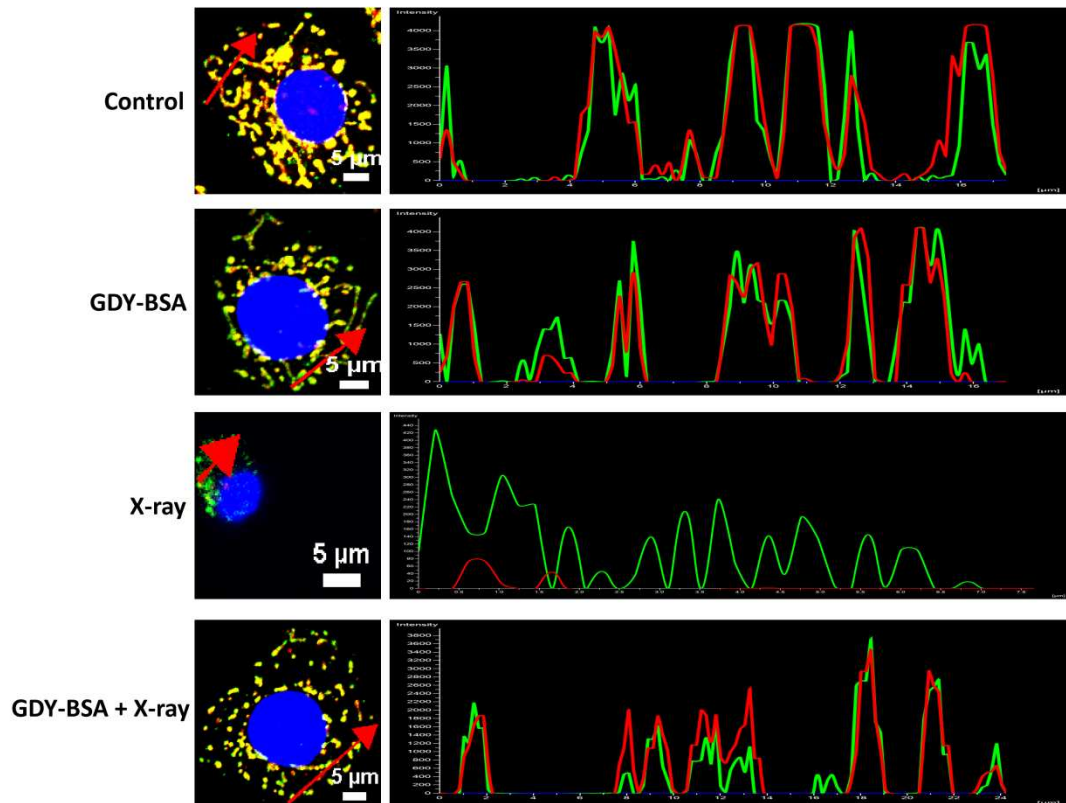
Fig. S11. The co-location of cytochrome c and mitochondria in IEC-6 cells after different treatments, which indicate the location of red arrow
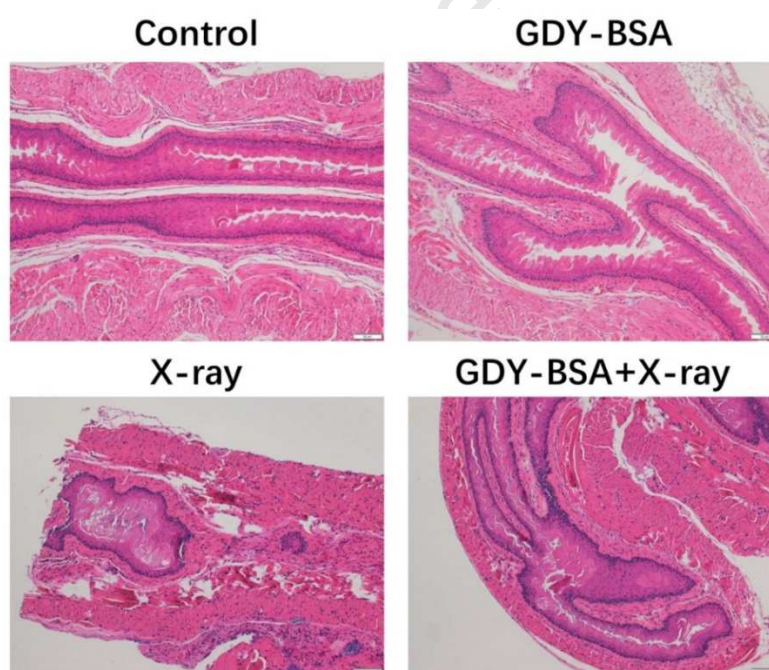
Fig. S12 The survival percentage of mice with time after different treatments. The oral drug dose of GDY-BSA NPs is 12.5 mg/kg.

Fig. S13 The minimum effective dose exploration. Histopathology analysis of mice after different treatments.
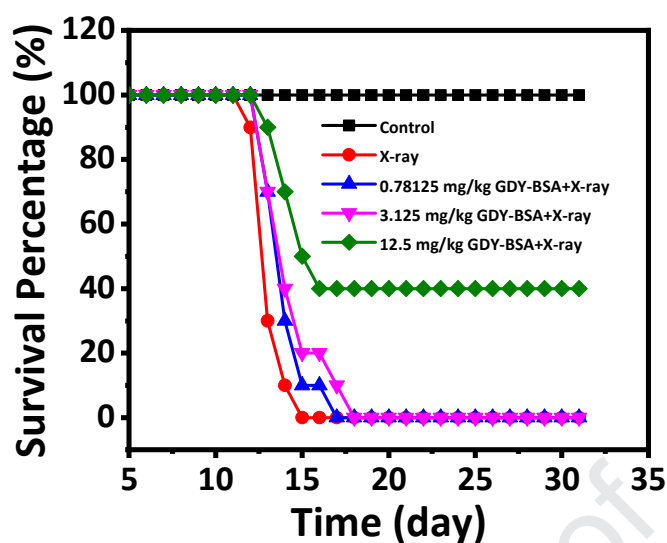
Fig. S14 The survival percentage of mice with different drug doses.

Fig. S15 The radioprotective effect of GDY-BSA NPs to esophagus. Esophagus is also a very important component in digestive tract, which possesses close relationships with gastrointestinal tract, we also observed the radioprotective effect of GDY-BSA NPs to esophagus.

Declaration of interests

The authors declare that they have no known competing financial interests or personal relationships that could have appeared to influence the work reported in this paper.